

Dynamic Model of a Piano Action Mechanism

by

Martin C. Hirschorn

A thesis
presented to the University of Waterloo
in fulfilment of the
thesis requirement for the degree of
Master of Applied Science
in
Systems Design Engineering

Waterloo, Ontario, Canada, 2004

©Martin C. Hirschorn, 2004

I hereby declare that I am the sole author of this thesis. This is a true copy of the thesis, including any required final revisions, as accepted by my examiners.

I understand that my thesis may be made electronically available to the public.

Martin C. Hirschorn

Abstract

While some attempts have been made to model the behaviour of the grand piano action (the mechanism that translates a key press into a hammer striking a string), most researchers have reduced the system to a simple model with little relation to the components of a real action. While such models are useful for certain applications, they are not appropriate as design tools for piano makers, since the model parameters have little physical meaning and must be calibrated from the behaviour of a real action.

A new model for a piano action is proposed in this thesis. The model treats each of the five main action components (key, whippen, jack, repetition lever, and hammer) as a rigid body. The action model also incorporates a contact model to determine the normal and friction forces at 13 locations between each of the contacting bodies. All parameters in the model are directly measured from the physical properties of individual action components, allowing the model to be used as a prototyping tool for actions that have not yet been built.

To test whether the model can accurately predict the behaviour of a piano action, an experimental apparatus was built. Based around a keyboard from a Boston grand piano, the apparatus uses an electric motor to actuate the key, a load cell to measure applied force, and optical encoders and a high speed video camera to measure the positions of the bodies. The apparatus was found to produce highly repeatable, reliable measurements of the action.

The behaviour of the action model was compared to the measurements from the experimental apparatus for several types of key blows from a pianist. A qualitative comparison showed that the model could very accurately reproduce the behaviour of a real action for high force blows. When the forces were lower, the behaviour of the action model was still reasonable, but some discrepancy from the experimental results could be seen.

In order to reduce the discrepancy, it was recommended that certain improvements could be made to the action model. Rigid bodies, most importantly the key and hammer, should be replaced with flexible bodies. The normal contact model should be modified to account for the speed-independent behaviour of felt compression. Felt bushings that are modelled as perfect revolute joints should instead be modelled as flexible contact surfaces.

Acknowledgements

I would like to thank my supervisors, Prof. John McPhee and Prof. Stephen Birkett for allowing me to work on this fantastic project, and for providing great support throughout.

I would also like to thank *Steinway and Sons*, New York, for collaborating on the project, and more specifically, Susan Kenagy for all her help.

The entire Motion Research Group was a great help throughout my student career in Waterloo. Vicky Lawrence has also been a welcome friendly presence in the department. Without her, I'd probably still be trying to find my lab.

Finally, I'd like to thank my family for their support, most notably my sister, Kristine, for proof-reading this thesis.

Contents

1	Introduction and Literature Review	1
1.1	Introduction	1
1.2	Action Design	3
1.3	Literature Review	5
1.3.1	Piano Action Modelling	5
1.3.2	Contact Dynamics	7
1.4	Contributions of this Thesis	9
2	Dynamic Model	12
2.1	Graph-Theoretic Method and <i>DynaFlexPro</i>	14
2.2	Contact Mechanics	17
2.2.1	Contact Detection	18
2.2.2	Normal Contact Model	19
2.2.3	Calibration of the Normal Contact Model	22
2.2.4	Tangential Friction Model	24
2.3	Regulation of the Piano Action	26
2.4	Numerical Solution of the Model	28
3	Experimentation	29
3.1	Equipment Setup	29
3.1.1	Actuation	29
3.1.2	Force Measurement	31
3.1.3	Position Measurement	32

3.1.4	Photography	33
3.2	Experiments	34
3.2.1	Actuation of Key	34
3.2.2	Force and Position Measurements	38
4	Results and Discussion	43
4.1	Forte Blow	44
4.2	Piano Blow	48
4.2.1	Contact Model with <i>Forte</i> Calibration	48
4.2.2	Contact Model with <i>Piano</i> Calibration	51
4.3	Double Blow	54
4.4	Sensitivity Investigations	56
5	Conclusions and Future Research	61
5.1	Conclusions	61
5.2	Future Research	62
	References	65
A	Model Parameters	67
A.1	Mass Properties	67
A.2	Geometric Properties	70
A.3	Contact Properties	73
A.4	Other Properties	74
B	Experimental Equipment	75

List of Tables

2.1	Contact Surfaces for Piano Action	18
A.1	Inertia Properties of Action Components	67
A.2	Geometric Properties of Ground	70
A.3	Geometric Properties of Key	71
A.4	Geometric Properties of Whippen	71
A.5	Geometric Properties of Jack	71
A.6	Geometric Properties of Repetition Lever	72
A.7	Geometric Properties of Hammer	72
A.8	Contact Properties	73
A.9	Rotational Friction Parameters	74
B.1	Software	75
B.2	Actuation Equipment	75
B.3	Load Measurement Equipment	76
B.4	Position Measurement Equipment	76
B.5	High-Speed Video Equipment	76

List of Figures

1.1	Piano Action	2
1.2	Schematic of a Piano Action	3
1.3	Three Bodies of the Simplified Piano Action	4
1.4	Five Bodies of the Full Piano Action	5
1.5	Modelling and Testing Process	10
2.1	(a) Felt Bushing on Whippen and (b) Balance Rail under Key	13
2.2	Simplified Graph of a Piano Action	15
2.3	Rotational Co-ordinates of the Action Model	16
2.4	Contact Locations of a Piano Action	17
2.5	Loading and Unloading Contact Forces	20
2.6	Loading, Unloading and Fit Curve Contact Forces	22
2.7	Piecewise and Smoothed Friction Curves	25
2.8	Key Points for Regulation of the Piano Action	27
3.1	Modified Keyboard with Key 52	30
3.2	Motor and Actuation Arm	31
3.3	Load Cell Mounted on Key	32
3.4	(a) MicroE Encoder and Scales (b) Encoder and Scale Mounted on Hammer	33
3.5	Experimental Setup	34
3.6	Measured Force Profiles by an Amateur Pianist	35
3.7	Pianist and Motor Force Profile for <i>Forte</i> Blow	36
3.8	Pianist and Motor Force Profile for <i>Piano</i> Blow	37
3.9	Measured Force for Five Trials with <i>Forte</i> Blow	38

3.10	Rotation of Key for Five Trials with <i>Forte</i> Blow ($\theta_k(0) - \theta_k$)	39
3.11	Rotation of Whippen for Five Trials with <i>Forte</i> Blow ($\theta_w - \theta_w(0)$)	39
3.12	Rotation of Hammer for Five Trials with <i>Forte</i> Blow ($\theta_h(0) - \theta_h$)	40
3.13	Rotation of Jack and Repetition Lever with <i>Forte</i> Blow ($\theta_j(0) - \theta_j, \theta_r(0) - \theta_r$)	42
4.1	Force Profile for <i>Forte</i> Blow	44
4.2	Experimental and Model Rotation of Key for <i>Forte</i> Blow ($\theta_k(0) - \theta_k$) . . .	45
4.3	Experimental and Model Rotation of Whippen for <i>Forte</i> Blow ($\theta_w - \theta_w(0)$)	46
4.4	Experimental and Model Rotation of Hammer for <i>Forte</i> Blow ($\theta_h(0) - \theta_h$)	46
4.5	Force Profile for <i>Piano</i> Blow	49
4.6	Experimental and Model Rotation of Key for <i>Piano</i> Blow ($\theta_k(0) - \theta_k$) . . .	49
4.7	Experimental and Model Rotation of Whippen for <i>Piano</i> Blow ($\theta_w - \theta_w(0)$)	50
4.8	Experimental and Model Rotation of Hammer for <i>Piano</i> Blow ($\theta_h(0) - \theta_h$)	50
4.9	Model Rotation of Key with Increased Damping for <i>Piano</i> Blow ($\theta_k(0) - \theta_k$)	52
4.10	Model Rotation of Whippen with Increased Damping for <i>Piano</i> Blow ($\theta_w -$ $\theta_w(0)$)	52
4.11	Model Rotation of Hammer with Increased Damping for <i>Piano</i> Blow ($\theta_h(0) -$ θ_h)	53
4.12	Force Profile for Double Blow	54
4.13	Experimental and Model Rotation of Key for Double Blow ($\theta_k(0) - \theta_k$) . .	55
4.14	Experimental and Model Rotation of Whippen for Double Blow ($\theta_w - \theta_w(0)$)	55
4.15	Experimental and Model Rotation of Hammer for Double Blow ($\theta_h(0) - \theta_h$)	56
4.16	Model Rotation of Hammer with Decreased Damping for <i>Forte</i> Blow ($\theta_h(0) -$ θ_h)	57
4.17	Model Rotation of Hammer with No Damping for <i>Forte</i> Blow ($\theta_h(0) - \theta_h$)	58
4.18	Model Rotation of Hammer with No Tangential Friction for <i>Forte</i> Blow ($\theta_h(0) - \theta_h$)	58
4.19	Model Rotation of Hammer with No Rotational Friction for <i>Forte</i> Blow ($\theta_h(0) - \theta_h$)	59
A.1	Defined Points on Action Components	68

Chapter 1

Introduction and Literature Review

1.1 Introduction

The invention of the piano is generally credited to Bartolomeo Cristofori, an Italian instrument builder, in 1697. The piano was created in an attempt to add dynamics (variable volume control) to another popular instrument at the time, the harpsichord.

The harpsichord is a large stringed instrument, where each string is tuned to a different pitch. Each string is actuated by a mechanism that plucks the string with a quill when a key is depressed. The musician has no way of altering how hard the quill plucks the string, so all notes are of the same volume. This was a serious drawback of the instrument, since most others at the time, such as violins and horns, allowed for varying dynamics.

In order to add dynamic control to the harpsichord, Cristofori replaced the quill mechanism with a key-actuated hammer. The harder the key is depressed, the faster the hammer moves, and the louder the resulting note. This name of the new instrument was the *gravicembalo col piano e forte* (harpsichord with loud and soft), but it was eventually shortened to *piano*.

The piano gradually gained in popularity to become one of the most widely played instruments in the world.

The mechanism that makes the dynamics possible is the piano *action*, as seen in Figure 1.1. The action transfers the force applied at the key front to the hammer, which in turn strikes the string. The functionality and design of the action are discussed in

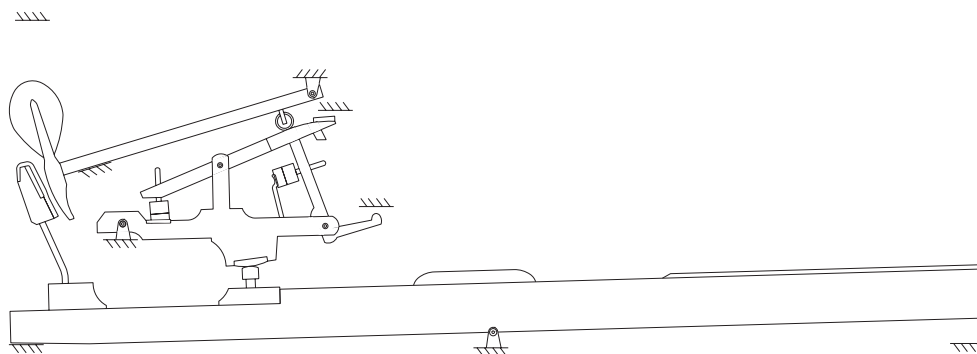


Figure 1.2: Schematic of a Piano Action

- How fast is the hammer moving for various intensities of finger blows on the key?

The purpose of this project was to create a model to simulate the behaviour of a piano action, and create an experimental apparatus to test real piano actions. A comparison between the behaviour of the modelled action and experimental action would provide an indication of how good the model is.

1.2 Action Design

While most piano makers design and build their own actions and claim certain advantages over others, all of the designs have the same basic shape, with only slight variations in dimensions and materials. For this reason, any discussion about the specific action in this thesis could also apply to any other modern piano action.

A schematic of a piano action is shown in Figure 1.2. During most of the key stroke, the action could be considered to have three rigid components, as shown in Figure 1.3.

A pianist presses on the front of the *key*. The centre of the key is resting on the *balance rail*, so a force at the front causes the key to rotate clockwise, which moves the *capstan* upwards. The capstan then presses into the bottom of the *whippen assembly*, causing it to rotate about its pin. The whippen assembly then pushes up the *knuckle* of the *hammer*, causing it to rotate and strike a string located above.

While this simple description is valid while the key is being pressed, an action has two other requirements. The first requirement is that it must have an *escapement*. If the

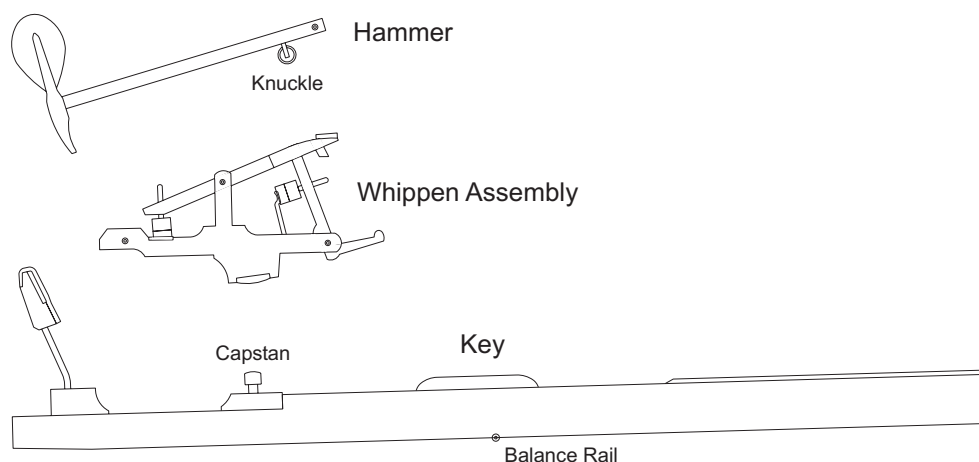


Figure 1.3: Three Bodies of the Simplified Piano Action

hammer were permanently connected to the key, it would be pushed and held against the string whenever the key was pressed, causing the note to be damped and muffled as it was struck. Instead, the hammer must be allowed to ‘escape’ when the key is depressed so it can freely strike the string and bounce away.

The second requirement is that the action must have a *repetition* mechanism, which allows repeated strikes. Once the hammer has escaped, it is no longer moving with the key. Releasing the key must re-latch the hammer, allowing successive strikes.

In order to achieve these two requirements, the whippen assembly is separated into three bodies: the *whippen*, *jack*, and *repetition lever*. This is shown in Figure 1.4.

The escapement is made possible by the jack. When the key is first depressed, the jack will be aligned between its own pivot on the whippen, and the knuckle on the hammer. This transmits all of the force from the whippen into the hammer. Once the hammer is nearly touching the string, the end of the horizontal arm of the jack (the *toe*) hits a small, fixed *button*, which causes the jack to rotate clockwise so that it is no longer pushing on the knuckle. This allows the hammer to fly free and fall back from the string while the key is still fully depressed. The hammer then catches on the *back check* (which has a high coefficient of friction) to prevent it from bouncing back up and re-striking the string.

The second requirement, repetition, is accomplished by the repetition lever. When the key is partially released after the note is complete, the hammer is released from the back

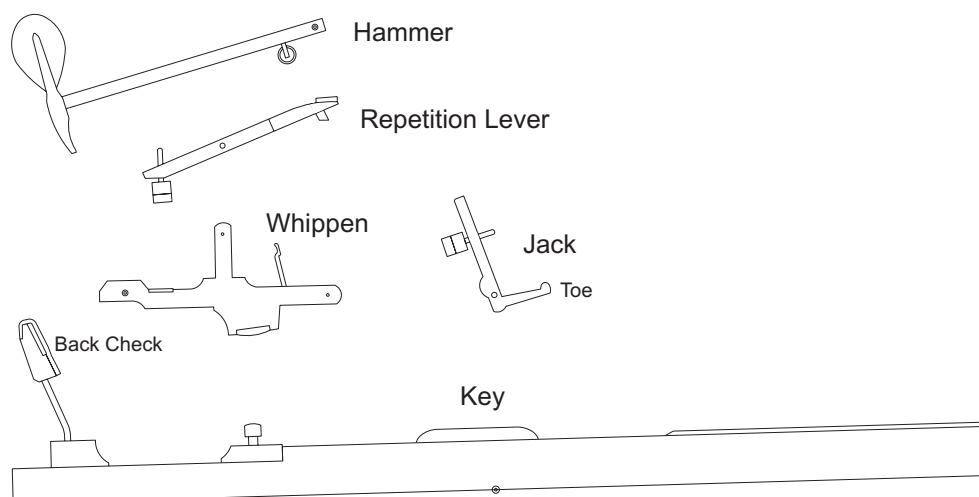


Figure 1.4: Five Bodies of the Full Piano Action

check and lifted by the repetition lever so it is held a few millimetres below the string. At the same time, the jack will move away from the button, allowing it to fall back under the hammer.

All of the main bodies of the action are made of various types of wood, though the large head of the hammer is felt. All contacting surfaces and bushings are lined with felt or leather to allow a softer feel and reduce mechanical noise in the action.

1.3 Literature Review

1.3.1 Piano Action Modelling

While the piano action has been largely ignored by multibody dynamics researchers, several musically-inclined engineers have performed some modelling of the action.

One of the first analyses of a piano action was performed by Pfeiffer in 1921, though an English translation was not available until 1967 [13]. Pfeiffer conducted extensive analytical investigations of various actions and components and identified how changes to certain parameters affect both the kinematic and kinetic the behaviour of the action.

One of the earliest attempts at modelling the piano action was made in 1937 by Matveev

and Rimsky-Korsakov (also a well known composer) [10]. The action was reduced to a simple one-dimensional system consisting of two masses connected with a spring. One mass represents the key and whippen assembly, the other represents the hammer.

This model was also investigated by Oledzki in 1972 [11]. After observing that the model results were qualitatively different than the behaviour of an upright piano action, he proposed replacing the constant mass of the key with a variable mass, which changes with the position of the key.

Topper and Wills [16] proposed a more advanced model in 1987 consisting of two rotating bodies connected by a spring. One body represents the key, the other represents the hammer, with the spring representing the compliance in the whippen.

Though the parameters in Topper and Wills's model were determined through direct measurements of the action components, they had to be recalibrated to obtain good agreement with experimental results on a real action. Once recalibrated, the model produced reasonable results for the down stroke of the action.

In 1992, Gillespie [5] modelled the action using four two-dimensional bodies representing the key, whippen, jack, and hammer. The model uses rigid bodies connected with kinematic constraints. In order to simulate the escapement, three different sets of constraints are used to simulate the phases of motion where certain bodies are no longer in contact. This model includes no friction, damping or compliance in the bodies.

In 1996, Gillespie presented a Ph.D. thesis [6] that greatly expanded on his previous work. In addition to a survey of many different methods of modelling a piano action, several features were added to his action model. A repetition lever was added to the original four bodies, completing the action, as well as a fourth possible set of kinematic constraints. Also, springs, damping, and friction were added in certain locations to account for the compliance of some of the contacts and bodies.

As Gillespie's model uses kinematic constraints to represent the contacts between the bodies, the system must detect when the bodies should be in contact and when they are separated, and change the constraints accordingly. This requires that the state of the system be stored and passed to a new set of equations every time a change in constraints is detected. This also limits the possible motion of the action, since a real action is capable of entering states that are not allowed by any of the sets of kinematic constraints. As

the system instantaneously transitions between different constraints, the contact points behave as either perfect constraints, or unconnected points, with no transition to allow for compliance.

A model created by Van den Berghe, De Moor, and Minten [2] in 1995 uses ‘macros’ for each of the five bodies of the action and bond graphs to simulate the system. The completed model consists of 37 second-order differential equations and 27 constraint equations. The model parameters are based on physical properties. In a later attempt to improve the computational efficiency of the model, a simplified model was created, which was then ‘trained’ to match experimental results.

In 1999, Hayashi, Yamane, and Mori [8] used an action model to help develop an automatic playing piano. This model was very similar to the one-dimensional model originally proposed by Matveev and Rimsky-Korsakov [10] in 1937. However, in addition to the two masses joined by a spring, this model includes a third mass resting on top of the other masses, which represented a hammer that is allowed to fly free from the rest of the system. The model also constrains the motion of the masses to represent the maximum travel of the bodies. While the model obtained good agreement with experimental results for the initial blow, it could not model any of the subsequent motion of the action.

1.3.2 Contact Dynamics

Investigating which contact model would be most suitable to model the compression of felt and leather would be a large project on its own. There is a huge amount of current research in contact mechanics, and felt and leather are particularly difficult due to their large compliance and nonlinear behaviour. A full review of contact models is beyond the scope of this thesis. However, it was still necessary to investigate some possible contact models in order to choose one to be used in the action model.

Gilardi and Sharf [4] provide a good survey of the various contact and friction models currently available. Contact models are divided into two groups: *discrete* and *continuous*.

Discrete contact models consider a contact situation to be instantaneous. They relate the state of the contacting bodies before and after contact using an impulse-momentum analysis. It is assumed that displacements and applied forces are negligible during the infinitesimal time of contact.

Continuous contact models, as the name implies, consider the effects of the bodies at all times during the contact period. Most often, they relate the normal contact force between the bodies to the penetration depth and rate.

Hunt and Crossley [9] introduced a contact model based on a nonlinear spring-damper. Gonthier et al. [7] proposed a continuous model for use in real-time simulations, which improved upon the work by Hunt and Crossley by redefining a parameter (the damping factor) so the model is accurate over a wider range of contacts. The model was able to provide reasonable results for several examples.

While the previously mentioned discussions have focused on general contact models, the main application for the research has been stiff, homogeneous materials such as steel. Nearly independent of that, a whole different train of research has been performed on cloth, wool, and fibre assemblies. This research was expected to be more appropriate for modelling the felt and leather contacts in the piano action.

Some of the earliest research into compression of textiles was performed by van Wyk [17] in 1946. Van Wyk proposed that the stiffness of wool is related to:

$$A = \frac{KYm^3}{\rho^3} \quad (1.1)$$

where K and Y are related to material properties, m is the mass of the sample, and ρ is the density. A is defined as being proportional to the ‘resistance to compression’, but the specific physical meaning is not clear.

Dunlop [3] attempted to provide more realistic results based on van Wyk’s work. Primarily, Dunlop wanted a model that exhibits hysteresis, which is absent from van Wyk’s work. Dunlop combined multiple spring and Coulomb friction elements in different structures in an attempt to account for the complex internal structure in the wool. Each spring element is based on the van Wyk Equation (1.1). In certain cases, the model produces qualitatively reasonable results, though the fact that it contains multiple elements makes it difficult to simulate. Also, the model parameters do not seem to have any direct relation to physical properties of felt samples.

The final model chosen for the project was based on the continuous model proposed by Hunt and Crossley [9], but used a spring term that was more accurately tuned to the behaviour of felt. The model by Gonthier et al. [7] improved on Hunt and Crossley’s

model by redefining the damping parameter based on conditions at the start of the contact. However, in a piano action, some bodies might be in contact for the whole simulation, so there is no definable start of contact.

1.4 Contributions of this Thesis

Component-based modelling has been a valuable engineering tool in many industries for decades. Being able to predict the behaviour of a complicated assembly using only the properties of the constitutive components allows important design decisions to be made without the expensive procedure of building prototypes. For example, a good model would allow an automobile designer to predict the handling of a new car by describing the details of the components, such as the tires, steering system, and suspension.

While this type of modelling is common and well-understood, the piano action introduces many complexities not seen in other models. The action is primarily made of wood, which is not as easily described as most engineering materials. Felt and leather are used between most of the components to give a softer feel and prevent noise as bodies interact. Rather than standard bearings or bushings, an action uses felt bushings, which have high friction and also allow a small amount of translational movement. Friction between the components varies drastically, as some are lubricated with graphite, and others are rough wood against leather.

Many of the previous researchers in piano modelling [11, 16, 8] used simplified models of the piano action whose parameters must be iteratively tuned so the results match the behaviour of the real action. By reducing the number of parameters required to define the model, the complexity and computational expense of the simulations can be reduced.

However, simplifying the model in that way removes any possibility of using the model as a design and prototyping tool. If the model is to accurately simulate a design that has not been built, it must only use the physical properties and dimensions of the constitutive components. There is no physical action to use to calibrate the model. Also, it is difficult to determine forces, speeds, and other useful measurements of interacting bodies if the bodies are lumped together.

As the model created for this thesis is primarily intended as a tool to assist the design

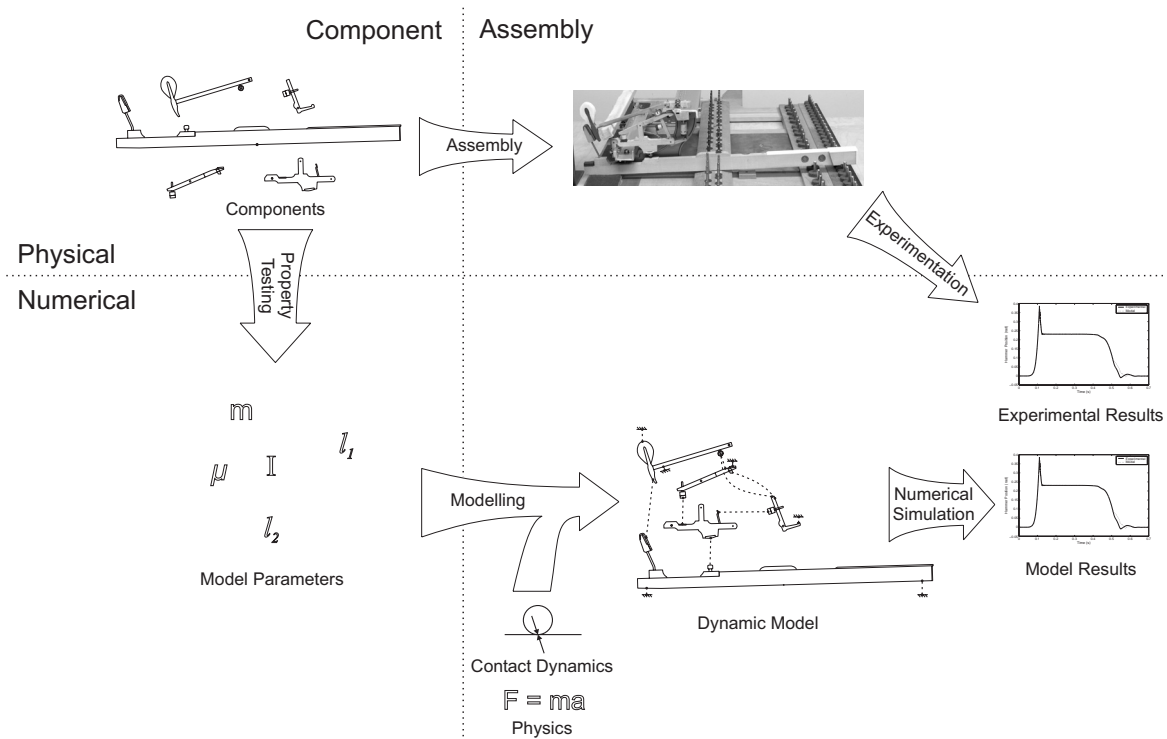


Figure 1.5: Modelling and Testing Process

and analysis of piano actions, it was designed to be mechanistic. All parameters and bodies in the model directly correspond to physical, measurable properties of the components comprising a piano action.

The result is a model that is intuitively understandable, can directly provide information about forces, speeds, and positions of any of the bodies in the system, and can accurately simulate new action designs simply by entering physical and geometric data.

In order to verify that the model produces accurate results, the model behaviour is compared to experimental results from a real piano action. The procedure for testing and comparison is depicted in Figure 1.5. Since all parameters used in the model are obtained from measurements of the components, completely independent of the assembled action, agreement between model and experimental results would indicate a valid model.

While it is beyond the scope of this project to create a model that accounts for all possible characteristics of the piano action, it is expected that reasonable results can be

obtained even with some simplification. Also, in completing the model it is hoped that some understanding can be gained into which effects are most important so that they can be more accurately incorporated into future models.

Chapter 2

Dynamic Model

While it is expected that a good action model should be valid for any style of action, a single action has to be chosen for the initial testing. In this case, the model was based on key 52 of a Boston model GP-178 grand piano. Key 52 was chosen because it is in a well-braced location on the keyboard. All physical parameters and geometric dimensions in the model were taken from this action.

It was decided that this model must closely resemble the physical action. However, there are certain characteristics and effects in the action that are insignificant or too complicated to accurately reproduce.

The first simplification made was that the motion of all bodies was assumed to be planar. This is reasonable, since a piano action is designed to prevent movement out of the plane.

Obviously the five main bodies, the key, whippen, jack, repetition, and hammer must be included in the dynamical model. It was decided to model the bodies as rigid. It is beyond the scope of this project to include all possible effects, and flexible bodies would significantly increase complexity and computational time required to simulate the system.

When first looking at the action, it appears the bodies are fixed to each other and to the frame with simple pin joints. However, most of the joints are felt bushings, as seen in Figure 2.1(a). This means that there will be some translational movement in the joints, as well as friction. One of the bodies, the key, is not connected to ground with a pin joint, but is resting on a felt washer on top of the balance rail. While a vertical pin prevents

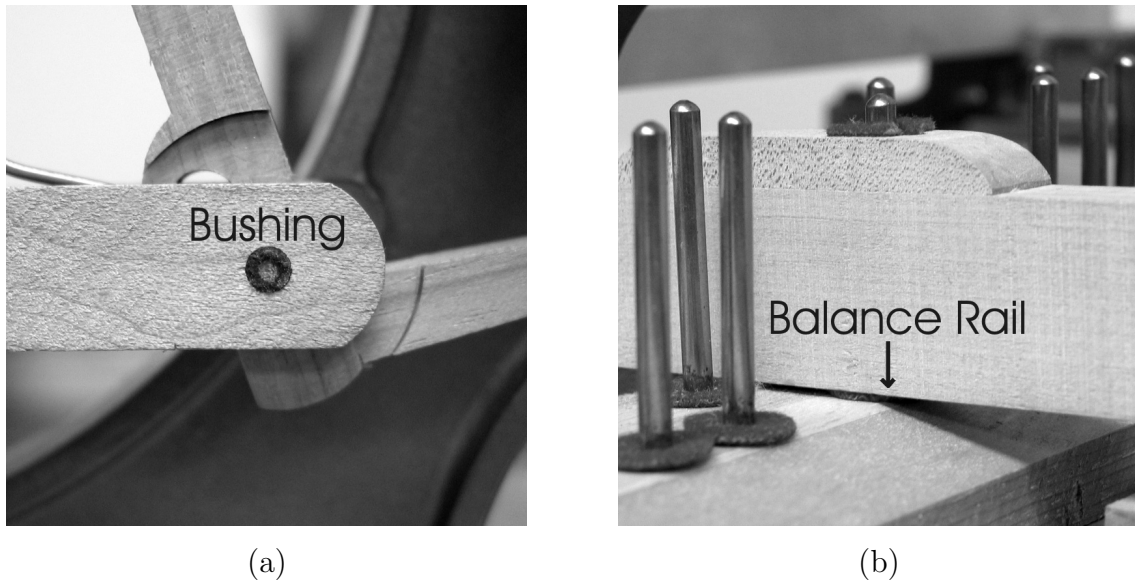


Figure 2.1: (a) Felt Bushing on Whippen and (b) Balance Rail under Key

horizontal movement, only gravity holds it down. This is seen in Figure 2.1(b). This behaviour was simplified by considering all joints as simple revolute joints, though friction was included in each. The modelling of these components is discussed in Section 2.1

The interaction between the bodies is a difficult situation to model. All contact points are padded with compressible felt or leather to prevent noise and vibration. Early in this project, a model was created that used kinematic constraints to represent the contacts between the bodies. While it produced reasonable results in some situations, it had significant limitations. The real contacts allow for the bodies to separate, but the model constrained everything together. It also did not include any compressibility in the contacts.

Instead, it was decided that the contacts should be treated as coupled applied forces. This is the *continuous* contact modelling approach discussed by Gilardi and Sharf [4]. The forces between each pair of contacting bodies are equal and opposite, and the magnitude and direction are calculated based on positions and velocities of the bodies. The chosen form of the contact model and how the collisions were detected is discussed in Section 2.2.

Once the final form of the model was chosen, the actual dimensions and properties

of the components were determined from measurements and experiments as discussed in Appendix A. The action and model then underwent a final regulation process (Section 2.3).

2.1 Graph-Theoretic Method and *DynaFlexPro*

The dynamic equations for a multibody system can be determined using many methods, such as *Linear Graphs*, *Bond Graphs*, or *Virtual Work*. It is not the purpose of this thesis to determine which method could most effectively model the system. The five bodies of the piano action comprise a fairly simple dynamic system that could easily be modelled with any method. Linear Graph Theory was chosen, since there is a large pool of expertise and automatic code generation tools available at the University of Waterloo.

Linear Graph Theory is a method that uses the topology of the system to determine the behaviour. A graph is created by describing the interconnections (*edges*) between all of the physical locations (*nodes*) in the system. Using a very methodical approach, the graph can be converted into a system of equations.

DynaFlexPro is a software package that uses Linear Graph Theory to automatically generate system equations for graphs. *DynaFlexPro* is built on top of *Maple*¹, and generates all equations in a symbolic form.

A partial graph of the system is shown in Figure 2.2. The first edges created in every graph are the rigid bodies, which account for the masses, moments of inertia, and gravitational forces on the bodies. Next, a rigid element must be added for every point of interest on the body. This allows the equations to describe the positions, rotations, and velocities of the specified locations.

In this model, the positions and velocities must be known for all contact locations in order to calculate the forces resulting from the contacts. These are shown in Figure 2.2 for the bodies, but are not shown for stationary, ground points to avoid making the figure too complicated.

The graph also includes edges for the joints connecting the bodies. In this case, there are revolute joints connecting the key, whippen, and hammer to ground. The revolute joints connecting the jack and repetition to the whippen also include rotational springs,

¹*Maple* is a software package produced by Waterloo Maple Inc.

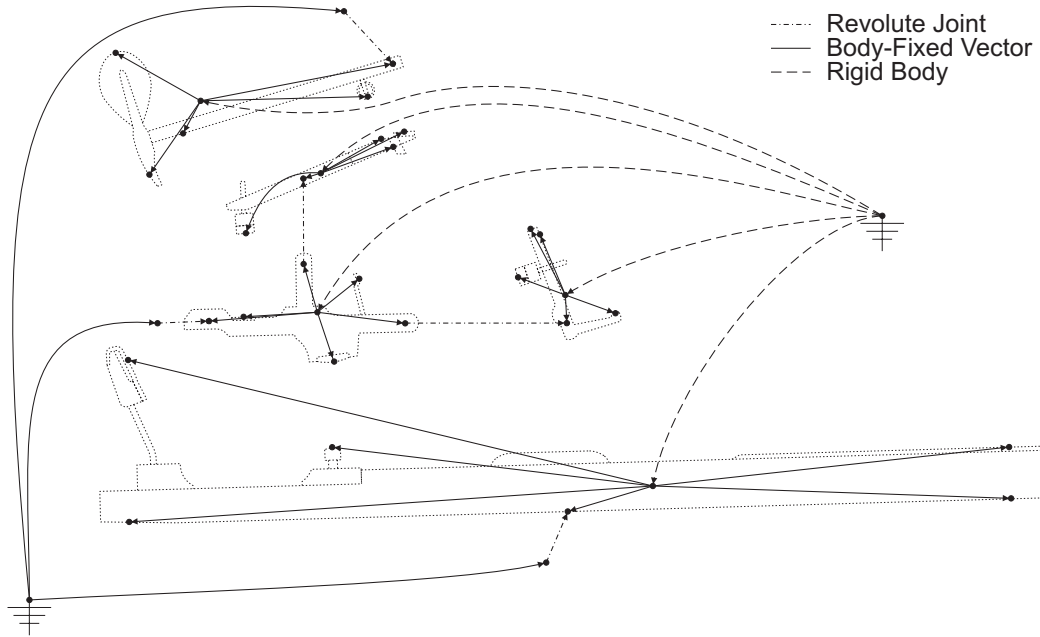


Figure 2.2: Simplified Graph of a Piano Action

which are present in the experimental action.

There are edges for the contacts between the bodies, but these would be too complicated to show in Figure 2.2 and are instead discussed in Section 2.2. There is also one applied force in the system. It is an externally specified force applied to the key front, which is used as the input variable.

The resulting system of equations produced by *DynaFlexPro* were reduced to include five system variables, as stored in the vector Q :

$$Q = \begin{bmatrix} \theta_k \\ \theta_w \\ \theta_j \\ \theta_r \\ \theta_h \end{bmatrix} \quad (2.1)$$

θ_k , θ_w , and θ_h are the rotations of the key, whippen, and hammer respectively, as measured counter-clockwise from ground. θ_j and θ_r are the rotations of the jack and repetition

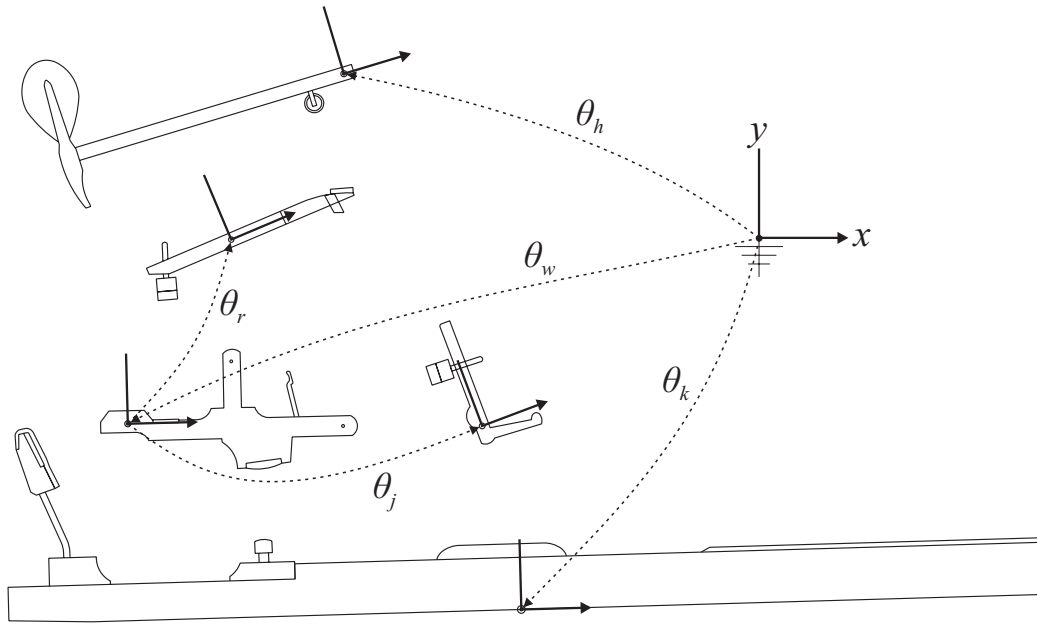


Figure 2.3: Rotational Co-ordinates of the Action Model

lever respectively, as measured counter-clockwise from the whippen. This is illustrated in Figure 2.3.

The set of five *Ordinary Differential Equations* (ODEs) produced by *DynaFlexPro* are of the form:

$$M\ddot{Q} = F \tag{2.2}$$

where M is the mass matrix of the system and F is a vector of quadratic velocity terms and forces applied to the bodies. As long as F is only a function of time (t), Q , and \dot{Q} , the equations can be solved with common ODE integrators.

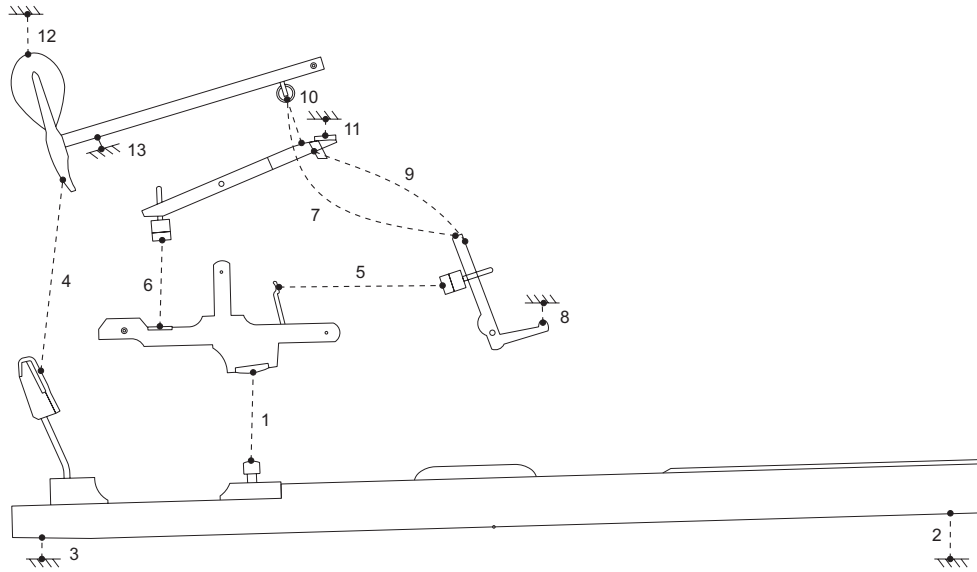


Figure 2.4: Contact Locations of a Piano Action

2.2 Contact Mechanics

The dynamic equations for the system were created by *DynaFlexPro* in *Maple*, but since the equations are highly nonlinear, they were exported to the *MATLAB*² programming environment where they were numerically integrated.

While many components, such as joints, rigid bodies, and springs were natively supported by *DynaFlexPro*, contacting surfaces were not. In order to include the contact forces in the dynamic equations, edges were added to the linear graph for each of the contacts. A special contact edge type was created in *DynaFlexPro* so that each contact surface calls a *MATLAB* function and passes it the position and velocity information of the two surfaces. The resulting forces and torques are calculated using the procedure outlined in the following sections, and are included in the F term of Equation (2.2). This contact edge was used for each of the 13 contacts in the piano actions, as shown in Figure 2.4.

²*MATLAB* is a software package produced by The MathWorks.

Contact	Description	Type
1	Key - Whippen at Capstan	Circle - Circle
2	Key - Ground at Key Front	Line - Circle
3	Key - Ground at Key Back	Line - Circle
4	Key - Hammer at Back Check	Line - Circle
5	Whippen - Jack	Line - Circle
6	Whippen - Repetition	Line - Circle
7	Jack - Hammer at Knuckle	Hybrid - Circle
8	Jack - Ground at Button	Circle - Line
9	Jack - Repetition	Line - Circle
10	Repetition - Hammer at Knuckle	Hybrid - Circle
11	Repetition - Ground at Stop	Line - Circle
12	Hammer - Ground at String	Circle - Line
13	Hammer - Ground at Rest	Circle - Line

Table 2.1: Contact Surfaces for Piano Action

2.2.1 Contact Detection

No matter what the final form of the contact model, it is necessary to perform contact detection. This determines whether the bodies are in contact based on the geometries of the contact surfaces and the positions of the bodies. Different geometries require different calculations, and for this project, three different possible geometries were allowed: circle, line, and a hybrid surface that consists of an arc with two lines extending tangentially from each end. It was found that these three shapes could reasonable represent all surfaces found in the action.

Table 2.1 lists and describes all 13 contacts and specifies which contact type was used. The geometry chosen for each contact does not affect the form of the calculation used to determine the contact force. It only determines whether the bodies are in contact, and the penetration depth. This means that certain contact types can be used in situations where they might not resemble the physical shape of the bodies. For example, the felt under the front of the key is actually a flat, horizontal disk, but treating it as a circular contact can

still produce the correct penetration depth. Since the key is connected to ground with a revolute joint and undergoes small rotations, the two contact points can be placed so that the circle contact moves nearly perpendicular to the plane.

Contact 12 in Table 2.1 represents the contact between the hammer and string. In a real piano, the string is capable of very complicated motion due to pulse waves travelling along the length. This behaviour would be very difficult to accurately simulate, so the string was replaced with a rigid, stationary body. This means that the results from the simulation can only be compared to experimental results with the hammer striking a solid body, not a string.

2.2.2 Normal Contact Model

While performing qualitative compression experiments on felt, several characteristics were observed:

Nonlinear Spring: The spring behaviour was found to be nonlinear. It also does not follow any simple power function.

Hysteretic: The behaviour of the felt at the current time depends on the previous state of the felt. The felt requires more force to compress than it returns on decompression. This results in energy loss through loading cycles.

Speed Independent: Whether the felt is loaded slowly or quickly seems to have little effect on the loading profile. Instead, it is dependent on the maximum and minimum loads the felt has previously undergone.

These characteristics can be seen in the loading profile of Figure 2.5

The Dunlop model [3], as discussed in Section 1.3.2, was initially considered for this project, as it is theoretically capable of producing all of the required characteristics. However, implementing such a model would cause many difficulties. For one, the Dunlop model is in the wrong form. It will produce a displacement for a known force, but for the action model with externally applied contact forces, it must produce a force for a known displacement. Also, there is as yet no reasonable way to calibrate the Dunlop model. It

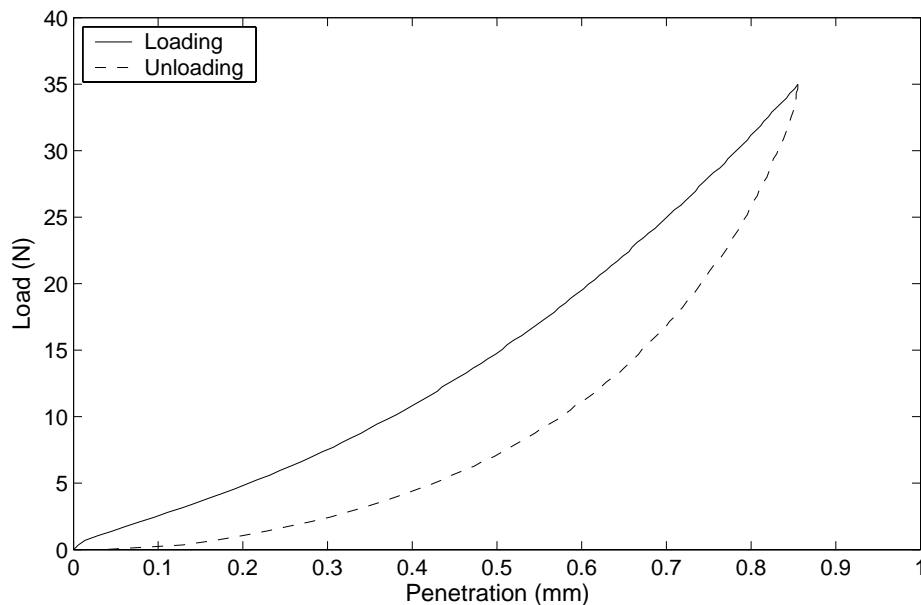


Figure 2.5: Loading and Unloading Contact Forces

is comprised of multiple spring and friction elements, but how the parameters in those elements relate to an actual felt contact is still unclear. Also, recent testing done by Stamm [14] in collaboration with this project has brought into question whether the model is capable of reproducing even Dunlop’s own experimental results.

The model proposed by Gonthier et al. [7] was also considered, but was rejected due to the fact that one of the key parameters, the damping factor, is determined from the initial contact velocity. This means the model can only be used in situations where the contact bodies are initially apart before making contact and rebounding. However, in the piano action, bodies can start in contact, and might stay in contact throughout the entire simulation.

An early version of the action model used a contact model based on the Hunt and Crossley [9] contact forces, as described in Section 1.3.2. The model was of the form:

$$f_n = kx^n(1 + D\dot{x}) \quad (2.3)$$

where f_n is the normal force, k is the spring constant, x is the penetration depth, n is the power of the contact (as determined from the geometry, usually 3/2), D is the damping factor, and \dot{x} is the normal velocity.

While it was known that this does not exactly match some of the known characteristics of felt contacts (such as speed independence) it was found to produce reasonable behaviour in the action model. The main discrepancy was that the power function for the spring force was not the same form as the actual felt profile.

The final contact model chosen for the project was similar to the Hunt and Crossley model, but the power spring function was replaced with a unique fit curve calculated from a loading profile that was experimentally measured for each of the contacts:

$$f_n = f_{fit}(x)(1 + D\dot{x}) \quad (2.4)$$

where $f_{fit}(x)$ is the force calculated from a third-order polynomial fit curve of the form:

$$f_{fit}(x) = ax^3 + bx^2 + cx \quad (2.5)$$

where a , b , and c are the polynomial coefficients determined using a least squares polynomial fit. These parameters for the contact model can be determined by performing a single loading experiment for each contact in the system.

Since the dynamic equations of the system are ODEs, it was preferred to keep the contact model in a form that would produce ODEs as the final equations. The selected normal force model meets this criterion, as the force calculated by the contact function (which appears in the force vector, F) is only a function of fixed geometry, position (x or Q), and velocity (\dot{x} or \dot{Q}).

The biggest weakness of this model is that the hysteretic damping behaviour is speed dependent, and it is known from previous research (Stamm [14]) that the behaviour of real felt is not. However, the effect of this discrepancy could be minimized by choosing a damping term (D) that produces accurate reaction forces at speeds similar to those seen in the piano action.

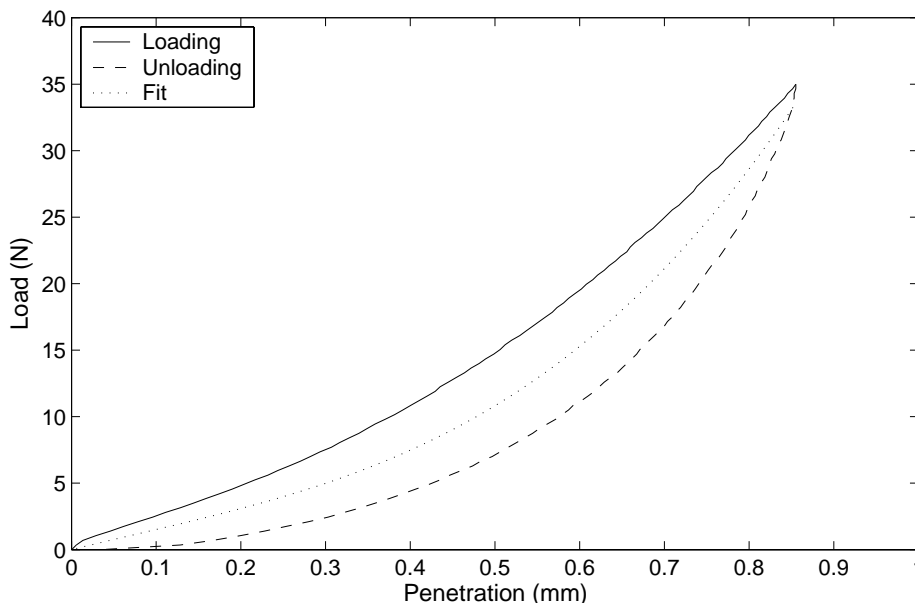


Figure 2.6: Loading, Unloading and Fit Curve Contact Forces

2.2.3 Calibration of the Normal Contact Model

The first step in determining the parameters to use in each of the contacts is to perform a loading experiment on each contact. This was done by disassembling the piano action, mounting one component in a vice and the other on a moving arm attached to a small motor. The torque output of the motor is controlled, and the rotation of the arm is measured with an encoder. This procedure isolates each contact and makes it possible to determine the displacement at each applied force for loading and unloading, as seen in Figure 2.5.

A third-order polynomial least-squares fit was then performed on the mid-line of loading and unloading curves to determine the coefficients of the fit curve of Equation (2.5). The loading, unloading, and fit curves for the contact under the key front are plotted in Figure 2.6.

This fit curve is the spring force for the contact model. As seen in Equation (2.4), if the contact is in the loading phase (positive speed, \dot{x}), the normal force will be larger than the fit curve. During unloading, it will be less.

While the actual contact curves are not dependant on normal speed, the contact model is. The damping parameters, D , were chosen in order to reduce the error in each contact caused by this discrepancy. The optimum D was found by solving Equation (2.4) for D , as seen in Equation (2.6):

$$D = \left(\frac{f_n}{f_{fit}(x)} - 1 \right) / \dot{x} \quad (2.6)$$

Using this relation, the model could be made to exactly match the measured force for some chosen position and speed. The position, x , was chosen as the point of the largest difference between the loading and fit curves (x_{max}). The actual normal force, f_n , was taken from the measured loading curve ($f_{loading}$). The normal speed, \dot{x} , was set to the average speed at the contact, \dot{x}_{ave} . This result of the substitutions yields:

$$D = \left(\frac{f_{loading}(x_{max})}{f_{fit}(x_{max})} - 1 \right) / \dot{x}_{ave} \quad (2.7)$$

The average normal speeds, \dot{x}_{ave} , were determined for each contact location from an experiment with the real action. Encoders were used to measure the rotations of the key, whippen, and hammer, and a high-speed video camera measured the rotations of the jack and repetition lever. The trial was performed with the *forte* force profile measured in Section 3.2.1. Using these rotational positions and velocities, along with the measured dimensions from the model action, relative speeds at the contact locations could be determined. This resulted in profiles of normal speeds for the whole time of the blow and release for each contact point. The averages of these profiles were then calculated and used for \dot{x}_{ave} , though those instances when the bodies were not in contact or were at rest were filtered out.

This results in a contact model that closely matches the behaviour of the real felt contacts, as it is fit to real contact curves. However, the accuracy of the model depends on the speed of the contacts. The significance of this dependence is investigated in Chapter 4.

There is one contact in the system that was not calibrated this way. The damping factor of contact 12, the ‘string’, was iteratively adjusted to produce approximately the correct rebound speed for the hammer. Since a proper string model was not part of this thesis, this contact was adjusted to be accurate so it would not invalidate the rest of the

results.

2.2.4 Tangential Friction Model

Tangential friction modelling is not the subject of this thesis, so a relatively simple friction model was chosen, based on Coulomb friction.

The Coulomb friction law states that if two bodies are in contact with no relative motion, a friction force exists that will resist any motion, as long as the force does not exceed f_t , as calculated in Equation (2.8):

$$f_t \leq \mu_s f_n \quad (2.8)$$

where μ_s is the static coefficient of friction and f_n is the normal force at the contact, as determined from Equation (2.4).

If there is motion between the bodies, the resisting friction force is determined from Equation (2.9)

$$f_t = \mu_k f_n \quad (2.9)$$

where μ_k is the kinetic coefficient of friction. Note that the friction force is not dependent on the magnitude of the tangential speed. It is only dependent on whether or not there is any tangential speed.

One common method of modelling Coulomb friction is to create a piecewise curve based on the tangential speed of the bodies, as seen in Figure 2.7, which approximates the behaviour of friction.

The coefficient of friction will linearly increase until it reaches the maximum static friction coefficient value when the tangential speed reaches the threshold velocity. This simulates the fact that when there is no (or very little) relative velocity between the surfaces, the friction force will oppose the motion up to the static coefficient of friction. Once the relative tangential speed exceeds the threshold velocity, the friction coefficient is reduced to the kinetic coefficient of friction.

As piecewise curves can cause difficulty in numerical simulations, a smoothed friction curve was chosen instead, based on the relation (slightly modified from Cull and Tucker

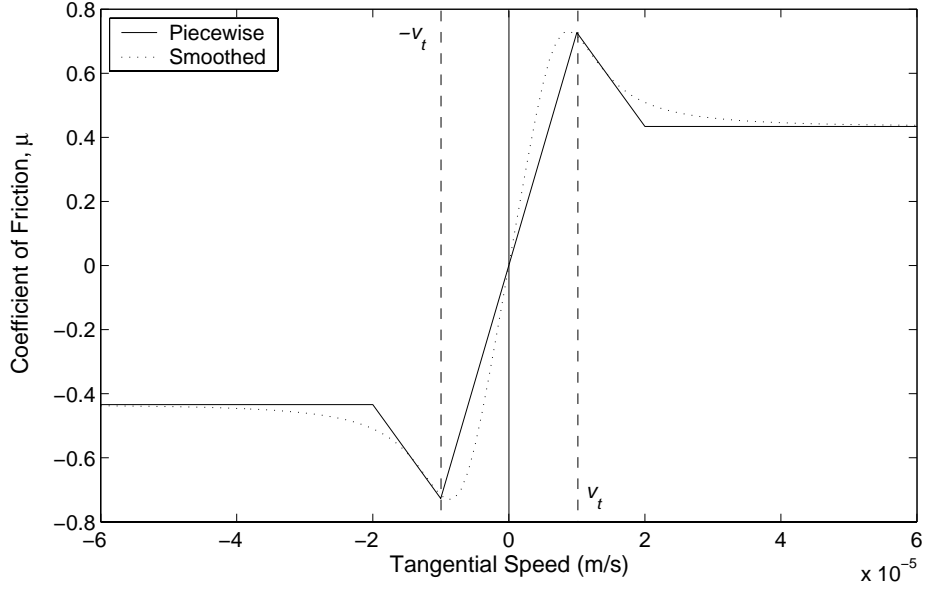


Figure 2.7: Piecewise and Smoothed Friction Curves

[1]):

$$\mu = A \left(\tanh(s_t/v_t) + \frac{B_1 s_t/v_t}{1 + B_2 (s_t/v_t)^4} \right) \quad (2.10)$$

where μ is the coefficient of friction, A , B_1 , and B_2 are constants that are determined from the static and kinetic coefficients of friction, s_t is the relative tangential speed of the two contacting surfaces, and v_t is the threshold velocity. A sample of this curve is also seen in Figure 2.7. The tangential friction force is then calculated from:

$$f_t = \mu f_n \quad (2.11)$$

When the relative tangential speed becomes large, the coefficient of friction approaches A . This means that the constant, A , is set to the kinetic coefficient of friction. B_1 and B_2 are manually adjusted so that the maximum peak of the curve matches the static coefficient of friction.

This smoothed Coulomb friction model was used for the four contacts that undergo significant tangential motion: 1, 4, 7, and 10 in Table 2.1. Tangential friction was ignored

for the other contacts, since the system constraints allow very little tangential movement.

A similar model was used for rotational friction in the five bodies. The same type of curve was used to relate the torque on the joint to the rotational speed of the body. The only difference is that the torque is not dependent on any normal force. The friction in the joints is primarily determined by the tightness of the felt bushings (ie., large pin in a small hole), which is constant once the action is assembled. This modified form is shown in Equation (2.12):

$$T = A \left(\tanh(\omega/\omega_t) + \frac{B_1\omega/\omega_t}{1 + B_2(\omega/\omega_t)^4} \right) \quad (2.12)$$

where T is the resulting torque, A , B_1 , and B_2 are constants determined from the measured torque in the joint, ω is the rotational speed, and ω_t is the threshold rotational speed.

2.3 Regulation of the Piano Action

Regulation is the process of making small adjustments to the piano action in order to maintain the proper feel and response. Piano actions are not always precisely manufactured, and will tend to change over time, since wood expands and contracts, and felt compresses and wears. In order to compensate for these changes, actions are designed with several adjustable components. For example, the capstan can be screwed in or out to adjust its height, washers can be placed under the key front to adjust the dip of the key, and the back check arm can be bent to change its position. This regulation process should be performed regularly on all pianos to maintain the proper response and feel. This process is outlined in Steinway and Sons [15].

Theoretically, if all of the measurements used in the model are taken from a properly regulated action, it should also be properly regulated. However, regulation adjustments are extremely fine, and are beyond the accuracy of any measurements. This is especially true for the location of the felt parts, since the ‘surface’ of the felt is not clearly defined. For this reason, the regulation procedure is also performed on the model after the geometry parameters of the components are determined.

The same procedure was used for both the experimental action and the model. The only difference was that the adjustments are made to the real action by turning screws or

7. The back check is adjusted by bending the metal wire connecting it to the key. Under a medium blow, the hammer should be stopped by the back check when the hammer height is 15.0 mm.

2.4 Numerical Solution of the Model

While *Maple* and *DynaFlexPro* were used to generate the code for the dynamic equations, the equations themselves were exported into *MATLAB*. All numerical solutions were calculated using the *MATLAB* ODE15s stiff solver with an absolute tolerance of 1×10^{-5} radians. A convergence study indicated that this error tolerance was sufficient to avoid inaccuracies or divergence in the results.

It was found that the solvers dedicated to stiff systems were much more efficient for this system. The contacts in the system are very stiff, with forces changing drastically with small variations in position. Even more significant in contributing stiffness is the friction model. While the smoothed model should be less problematic than the piecewise curve, it still exhibits very large changes in force for small changes in position and speed.

A full simulation for the system with a single force profile input requires about 6 minutes on a 2.4 GHz PC computer. *MATLAB* routines are known for their flexibility, not their performance, so the time could be significantly decreased by implementing the model and solvers in a dedicated, compiled language.

The model solution is compared to experimental results in Chapter 4.

Chapter 3

Experimentation

3.1 Equipment Setup

The experimental setup is based around a keyboard from a Boston GP-178 grand piano. In order to mount equipment, the keyboard was stripped to a single key and the rails were cut down to just one section. This allows access to the key and still maintains a very rigid frame. All experiments were performed on key 52, as it was in a position on the keyboard that allowed easy instrument access, but was still rigidly supported.

As discussed in Section 2.2.1, modelling a string would be very complicated so the string was replaced with a solid contact in the action model. In order to maintain similar behaviour with the experimental apparatus, the piano string was replaced with a solid metal bar. The modified keyboard can be seen in Figure 3.1.

In addition to the keyboard, there are four main components in the experimental system: actuation, force measurement, position measurement, and photography. Equipment suppliers and part numbers are listed in Appendix B.

3.1.1 Actuation

While a piano is normally played by a person, having a human actuate a system for experiments would provide unrepeatable results. Even though experienced pianists can closely duplicate piano blows, the consistency would be much better with a mechanical

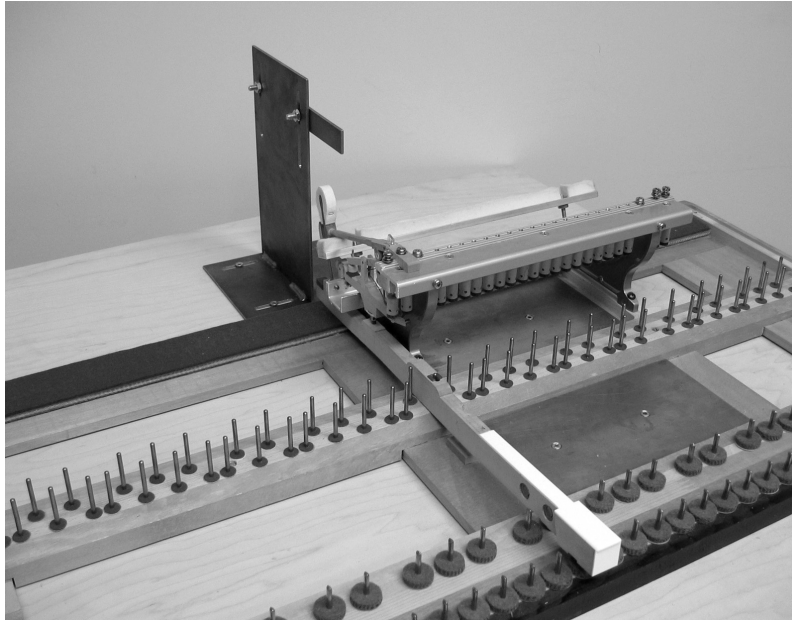


Figure 3.1: Modified Keyboard with Key 52

actuator.

Initially a linear motor was considered for the experimental system. A linear actuator is similar to a brushless motor with the coils unwound so that it creates a perfectly linear motion. It was thought that a straight motion would be desirable to actuate the key. However, a linear motor has several drawbacks. The first is that they are several times the price of a rotary motor of similar power. The second is that the motors do not have very high accelerations due to the mass of the carriage (the moving part of the motor). The final problem is that when mounted vertically, the weight of the carriage is continually pulling down, requiring counter balance or active control to maintain the position.

Instead, a DC brushless rotary motor was chosen, a Kollmorgen MT308A1. By attaching a small interchangeable aluminium arm to the output shaft, the rotary motion of the motor can be converted to linear motion for small rotations. This setup is seen in Figure 3.2.

With the chosen arm length of 100 mm, the motor is capable of generating peak forces up to 120 N. This was considered adequate, as previous literature ([8], [12]) has tested

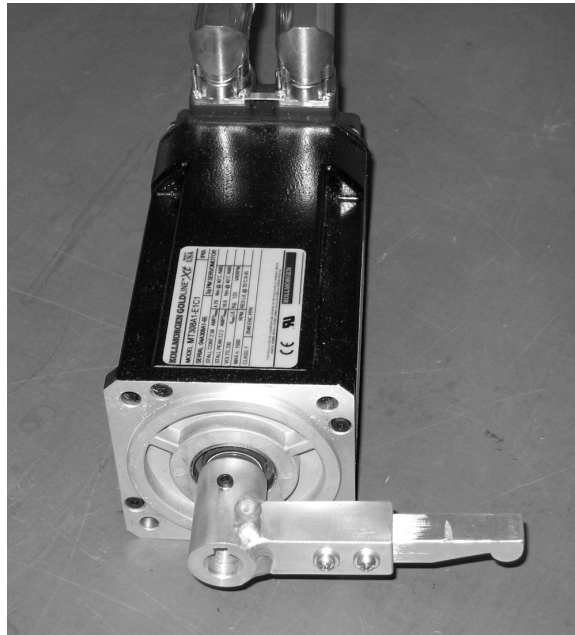


Figure 3.2: Motor and Actuation Arm

actual pianists' finger forces and found that they do not exceed 50 N.

The motor was controlled by a National Instruments PCI-7342 Motor Control board.

3.1.2 Force Measurement

The system also includes force measurement at the key front, since this was chosen as the input variable in the action model. In order to accurately measure this force, a 25 lb (111 N) rated subminiature load cell was purchased, a Sensotec model 13. The load cell is small and light enough (1.1 g) to be insignificant when added to the key. Samples were taken from the from the load cell up to a rate of 5000 Hz. The load cell was fastened to the key front using an adhesive strip, as seen in Figure 3.3.

The load cell uses strain gauges to measure the applied force, for which a National Instruments SCXI-1520 strain measurement system was used.

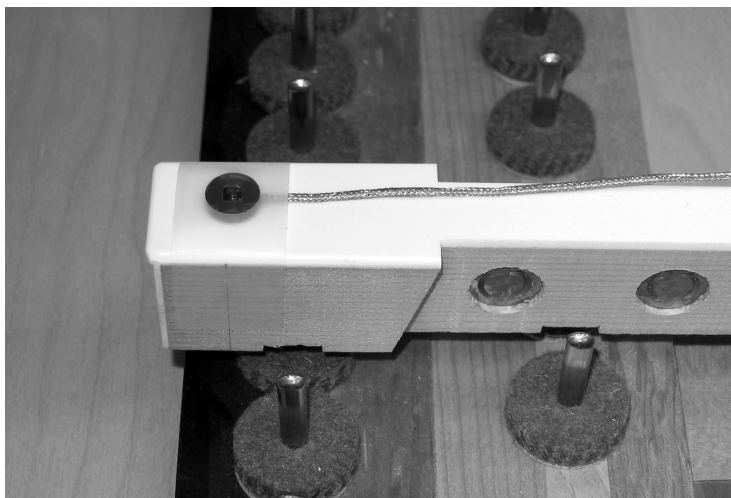


Figure 3.3: Load Cell Mounted on Key

3.1.3 Position Measurement

Initially, standard rotary encoders were considered for the rotary position measurements of the bodies in the system. These are small cylindrical devices with a rotating shaft mounted with bearings in the body. Inside the device, a disk-shaped scale with radial lines on it passes over an optical sensor, which counts how far the disk has rotated. However, there was a concern that the encoders would be difficult to mount on the action components. They would also add a significant amount of mass and friction to the system, since the encoder shaft must be affixed to the rotating body.

Instead, a modular encoder system was used. MicroE Systems makes a series of encoder optical sensors that can be used in conjunction with different shaped scales. The encoders and scales are not physically connected, so there is no friction added to the system. The optical sensors are mounted on fixed stands, and only the small scales are attached to the bodies in the system.

As there was not a lot of room surrounding the pins in the piano action, the rotary disks were cut into smaller arc segments. The arc segments and optical sensors can be seen in Figure 3.4(a). An arc segment was affixed at the pins of the key, whippen, and hammer, and the optical sensor was mounted in front, as shown in Figure 3.4(b). The arc centre

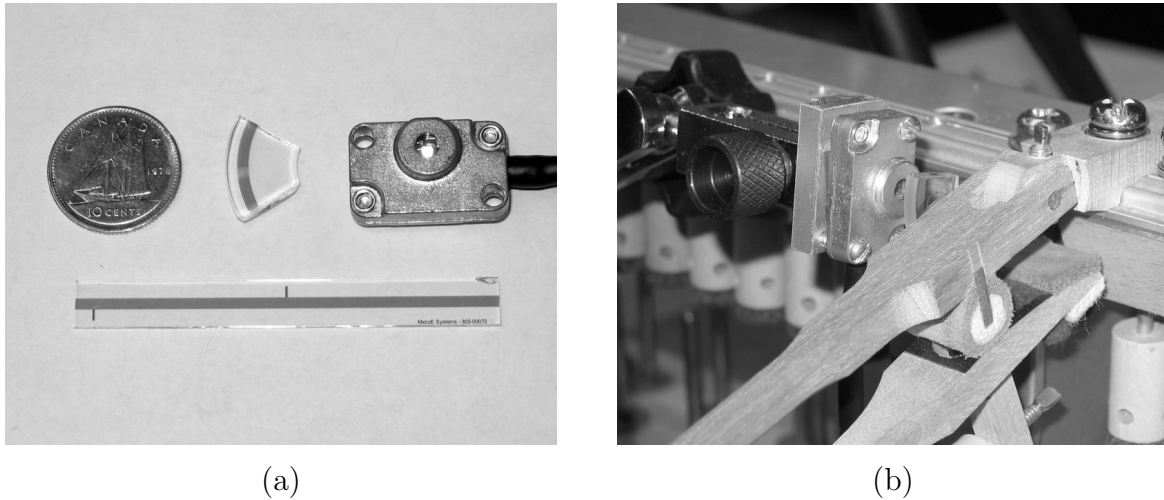


Figure 3.4: (a) MicroE Encoder and Scales (b) Encoder and Scale Mounted on Hammer

was placed at the centre of the pin with the aid of a small disk with the same radius as the arc segment.

This system is very useful for measuring the rotational position of the three bodies that are pinned to the frame of the piano, but can not measure the position for the jack and repetition without interfering with the behaviour of the system. The jack and repetition lever are pinned to the whippen, so the bodies' centres of rotation are moving and can not be measured with a fixed optical sensor. Measuring the rotations of these two bodies would require that the optical sensors be mounted on the whippen, which would add a significant amount of weight to the system.

The optical sensors are connected to small processors that interpolate the readings and send out a quadrature encoder signal. The quadrature signal is measured by a National Instruments PCI-6602 Counter/Timer board. The encoder system is capable of resolutions of 163,840 or 327,680 counts per revolution (depending on the scale diameter).

3.1.4 Photography

A high speed digital video camera was also used for the experiments, a Photron Fastcam-X 1280. The camera is capable of capturing high speed videos at resolutions up to 1280 by

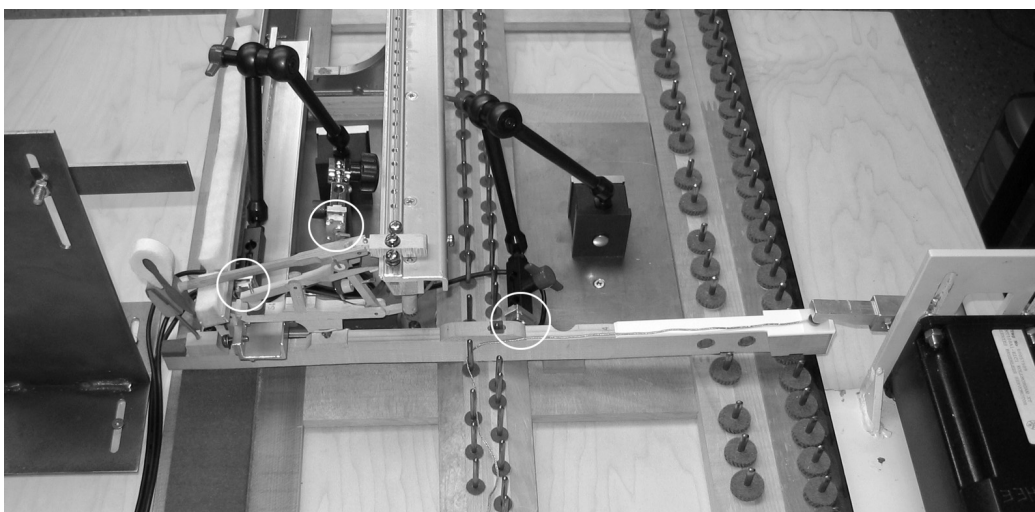


Figure 3.5: Experimental Setup

1024 pixels and speeds up to 16,000 frames per second, though the higher frame rates are only possible with lower resolutions. By interchanging lenses, the camera can be zoomed out to show the entire action, or zoomed in to a small ($10\text{ mm} \times 10\text{mm}$) area.

The camera included analysis software that can track points in the videos and report the position for each frame. While this is useful to get readings on components where an encoder could not be mounted, the resolution of the data is limited by the resolution of the video. There is a trade-off with using a small field of view that allows measurement of small movement, since that also reduces the distance a point can be tracked. Also, using the analysis software was time-consuming.

The experimental setup with motor, load cell, and encoders (circled) attached is shown in Figure 3.5.

3.2 Experiments

3.2.1 Actuation of Key

The first step in actuating the key is to measure the forces that occur at the key front when played by a pianist. Figure 3.6 shows five force profiles measured at the key front as played

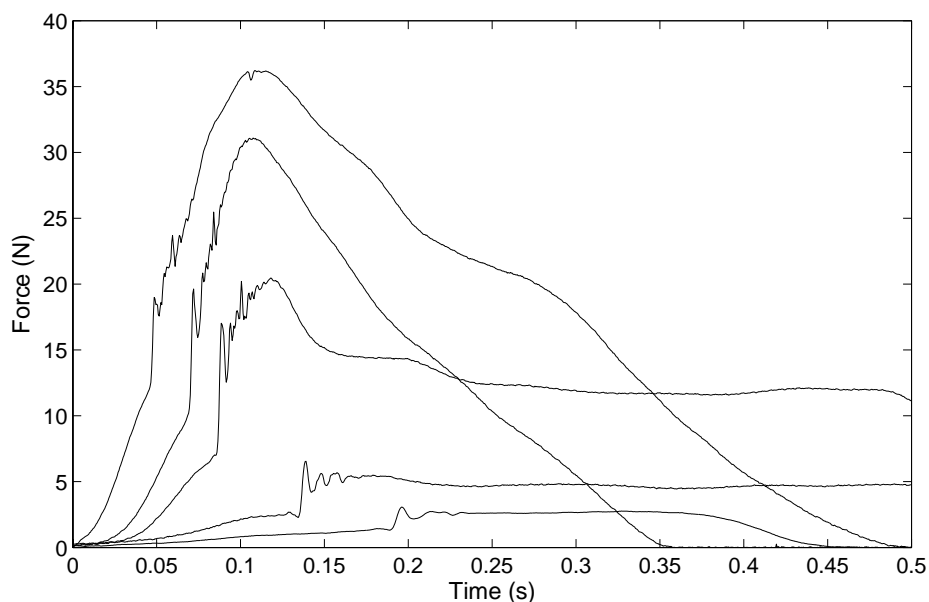


Figure 3.6: Measured Force Profiles by an Amateur Pianist

by an amateur pianist. All five blows were played *legato* style (with the finger in contact with the key from the beginning), with forces ranging from *piano* (soft) to *fortissimo* (very loud).

In all cases, the force gradually increased, then spiked suddenly when the key hit the key bottom. Any behaviour after this point is purely dependent on what the pianist chooses to do. The note might be held for a time, or released quickly.

As these profiles represent the actual forces that exist at the key front while the piano is played, they provide a good guideline for the force profile to use in the experiments. The experiments could be validly performed with any force profile, as long as the same profile was used in the simulated model, but mimicking these measured force profiles ensures that the action is tested in conditions that exist during normal use.

In order to test the model and experimental action over the full range of possibilities, two force profiles were used for the trials. One increases to 10 N, then spikes to 32 N, which will be referred to as *forte*. The other, *piano*, increases to 1.5 N, then spikes to 3 N.

Motor output profiles were created to reproduce these force profiles. The motor output

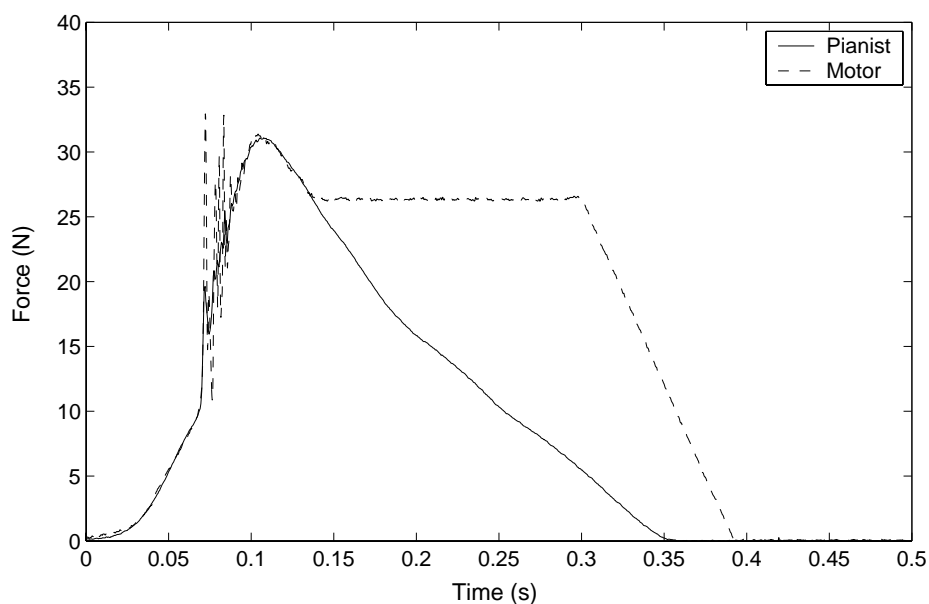


Figure 3.7: Pianist and Motor Force Profile for *Forte* Blow

profiles consist of lists of key points, and the motor output is interpolated at all instances in between. The profiles were created by scaling the measured pianist profiles to the equivalent motor output, then manually modifying the points to improve the accuracy. Figures 3.7 and 3.8 compare the profiles created by the pianist and motor.

In both cases, the motor profile spikes higher than the pianist profile when the key hits the bottom. This is due to the fact that the motor arm is a much harder material that does not have the compliance of a pianist's finger and arm. For the motor, all of the momentum in the stiff arm and motor shaft must be countered by the resisting force in the key, while a pianist's finger and arm will softly absorb the momentum. While it might be possible to reduce this spike by adding a compliance between the arm and key, this would increase the complexity of modelling the system.

The *forte* figure shows that the motor force was held on the key longer than the pianist. This is not accidental, but was an intentional decision to hold the key longer than the pianist to simulate a sustained note.

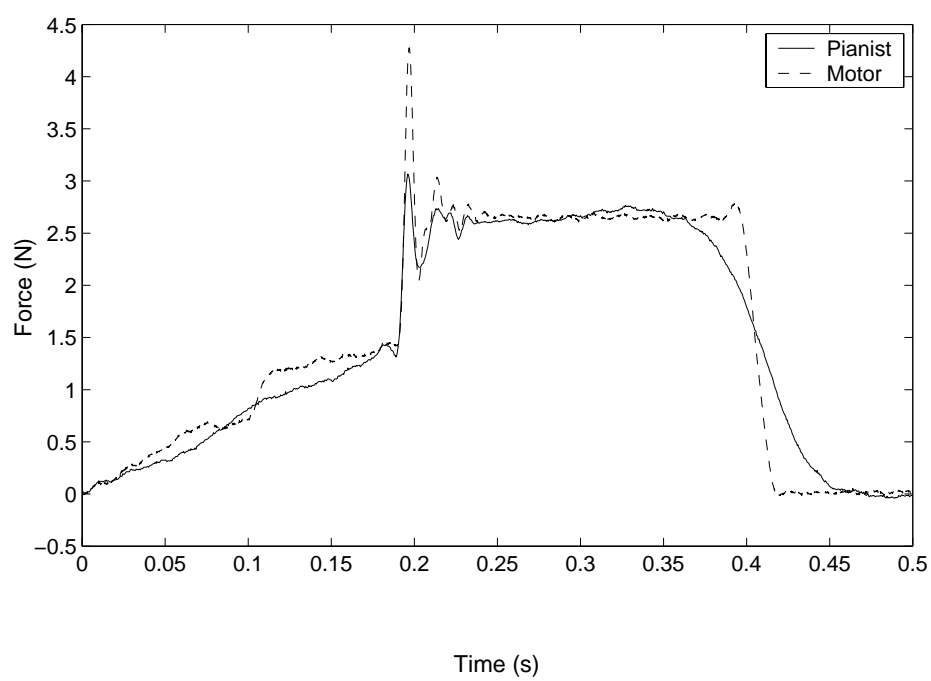


Figure 3.8: Pianist and Motor Force Profile for *Piano* Blow

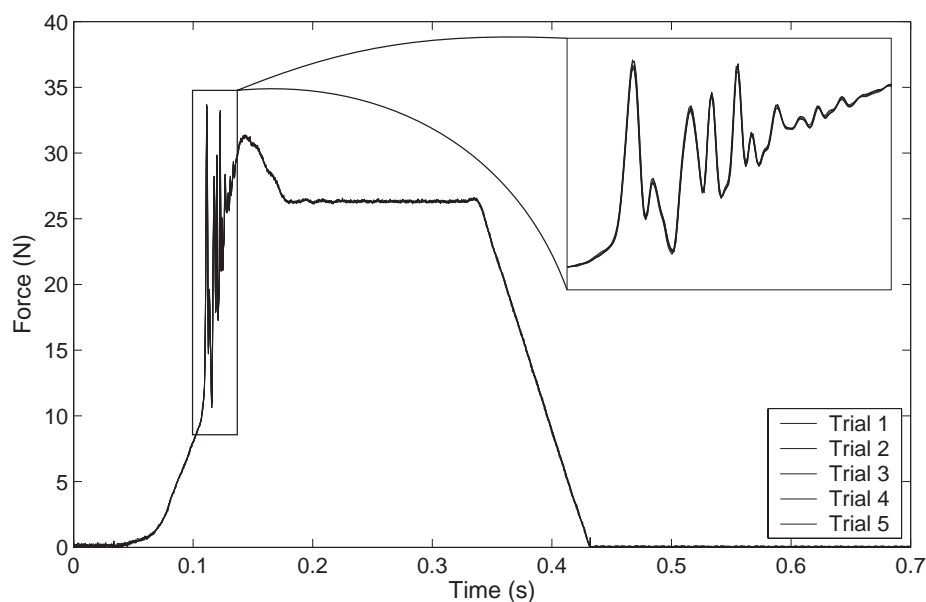


Figure 3.9: Measured Force for Five Trials with *Forte* Blow

3.2.2 Force and Position Measurements

In order to verify that the experimental setup is capable of producing consistent, repeatable results, five trials were performed for the *forte* force profile. The measured load for those five trials is shown in Figure 3.9.

The force profile for the five trials is virtually identical. Even the time between 0.11 and 0.13 seconds, which looks like noise, is the same between all trials. This indicates that the motor and controls are capable of producing very consistent force profiles. The positions of each of the three measured bodies for the five trials can be seen in Figures 3.10, 3.11, and 3.12.

As with the applied force, the positions of the bodies for the five trials are nearly identical. This inspires confidence that the experimental setup is capable of producing reliable, consistent results.

A short explanation of the motion of the action throughout the keystroke should make it easier to understand the following discussions. There are three positions labelled on the figures: *A*, *B*, and *C*.

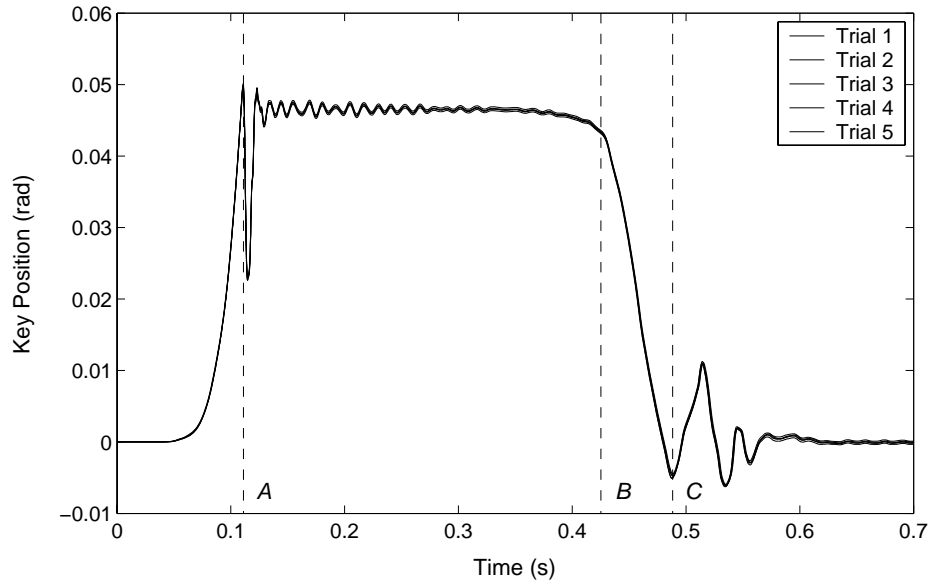


Figure 3.10: Rotation of Key for Five Trials with *Forte* Blow ($\theta_k(0) - \theta_k$)

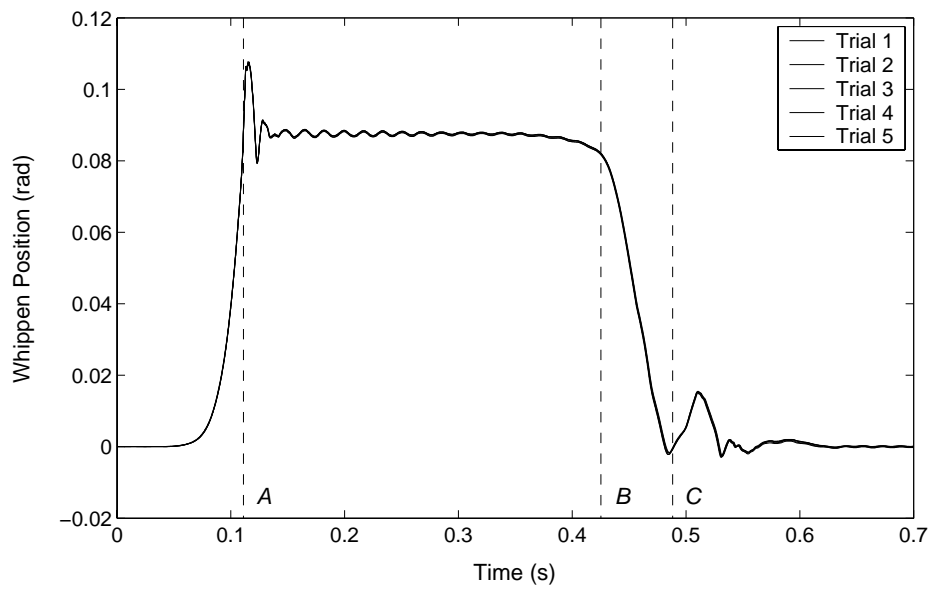


Figure 3.11: Rotation of Whippet for Five Trials with *Forte* Blow ($\theta_w - \theta_w(0)$)

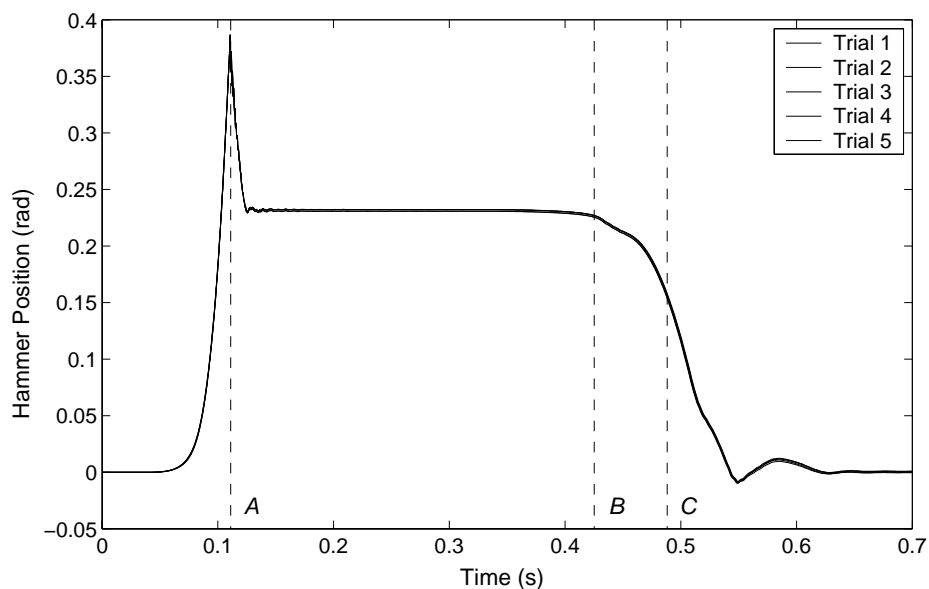


Figure 3.12: Rotation of Hammer for Five Trials with *Forte* Blow ($\theta_h(0) - \theta_h$)

Before Position *A*, the key is depressed and the action accelerates with the hammer moving toward the ‘string’. At *A*, the key reaches the key bottom, the action escapes, and the hammer flies free and strikes the ‘string’. These events happen at nearly the same time. Shortly after, the hammer rebounds off the ‘string’ and is caught by the back check.

The force is held on the key for a while, then starts to decrease shortly before *B*, until it is completely released at *B*. At this point, all components of the action start to fall back to their rest positions.

The key and whippen reach their lowest point at *C* and bounce several times. The hammer falls slightly slower, and does not fall back onto the whippen assembly until shortly after *C*.

A suspicious feature was noticed in the key rotation once it reaches its bottom at *A*. The experimental results show a large downward spike, which is questionable. This would indicate that the key bounces halfway back up after it hits the bottom. This would be significant enough to notice while playing the piano, but it does not happen. Also, a spike of this magnitude should be visible on the whippen, which is resting on the key.

This discrepancy was investigated with high speed video, and found to be an erroneous

reading by the optical encoders. It was assumed that the key could be accurately modelled with a revolute joint connected to ground, but it is in fact simply resting on the balance rail with a brass pin to prevent it from sliding sideways. While it was not expected that the key would lift off the balance rail, there is nothing preventing it from doing so.

By observing the key at the rail with high speed video, it was found that while the key was solidly on the balance rail for most of the blow, it was in fact lifting at certain times. There was a significant lift when the key front hit the bottom at *A*, as the momentum in the back of the key caused it to bounce up, which corresponds to the spike observed in the graph. Since the encoders depend on a rotary scale positioned around a centre point, any change in the centre causes an error in the reading.

While watching the video, it was also observed that the key lifted from the balance rail a smaller amount three other times later in the blow. This is observed in the key rotation graph (Figure 3.10) in the three low spikes at and shortly after *C*. At these times, the key back had reached the bottom, and the momentum of the key front caused it to lift and bounce three times. As with the earlier lift, this causes erroneously low readings in the key rotation measurement. The three bounces do exist, but the readings spike lower than they should.

A trial was also performed with the high speed video camera recording the position of the jack, and another with the position of the repetition lever. Using optical tracking on the videos, the rotational positions of the bodies were calculated, which are seen in Figure 3.13.

The data from the captured video is not as good as that from the encoders on the other three bodies. The video resolution is not sufficient to allow high resolution in the final data, which results in noticeable steps on the plot.

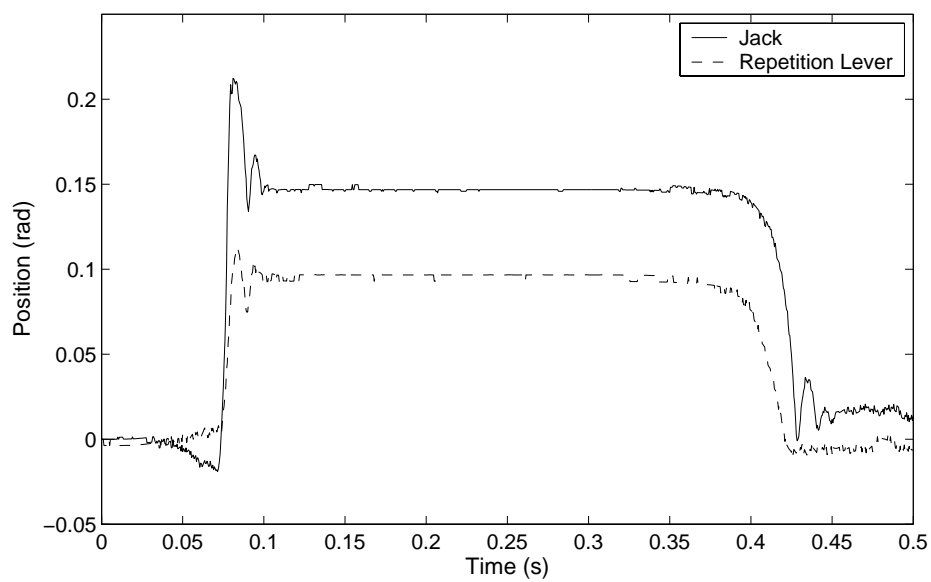


Figure 3.13: Rotation of Jack and Repetition Lever with *Forte* Blow ($\theta_j(0) - \theta_j$, $\theta_r(0) - \theta_r$)

Chapter 4

Results and Discussion

By measuring the actual force applied at the key front by the motor in the experimental trials in Section 3.2.1, force profiles were generated for the two different blows, *forte* and *piano*. A third force profile was also created by using two *forte* blows in rapid succession. In order to test whether the behaviour of the model is accurate, these force profiles were used in the model simulations to run trials that could be directly compared to the experimental results.

It should be noted that the measured force profile is not a completely independent, controlled variable. The force measured by the load cell at the key front depends on the behaviour of the actuating motor, as well as the dynamics of the experimental action. This causes some characteristics in the force profile that are not intentional, but are present because of the interaction of the actuation system and action. For example, there is a large force spike when the key front reaches the bottom, caused by the momentum of the motor arm pressing on the key.

An independent input variable would be preferred, since it would allow more precise control over the input to the system. However, that would require using a different variable as the input, such as the motor current, and modelling the actuation system in addition to the piano action.

The model has all five bodies of the system simulated. However, comparisons are only made of the positions of the key, whippen, and hammer, since the experimental results for these three bodies are more reliable than those for the jack and repetition lever.

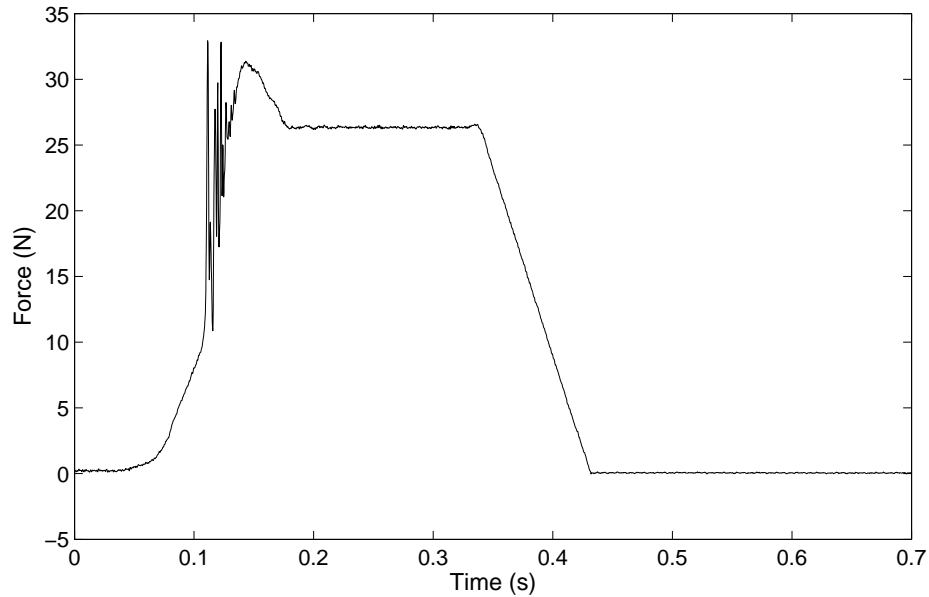


Figure 4.1: Force Profile for *Forte* Blow

A comparison of the experimental and model results is presented in the following sections.

4.1 Forte Blow

The force profile used for the *forte* blow is shown in Figure 4.1, which is simply the first trial that was plotted in Figure 3.9. The profile was measured from the actual experiment described in Section 3.2.1. The force starts at 0 Newtons, then from 0.05 to 0.11 seconds, gradually increases to 10 N. At this time, the experimental action reached the key bottom, which caused the force to spike up to about 34 N. The force is held for about 0.20 seconds, then eventually reduced to 0 again.

This force profile was imported into the action model as a table of 3500 times and forces (5000 Hz for 0.70 seconds). The force applied at the key front in the model was then linearly interpolated from the table for each time step, since the variable time steps used by the solver did not correspond to the fixed rate of measurements.

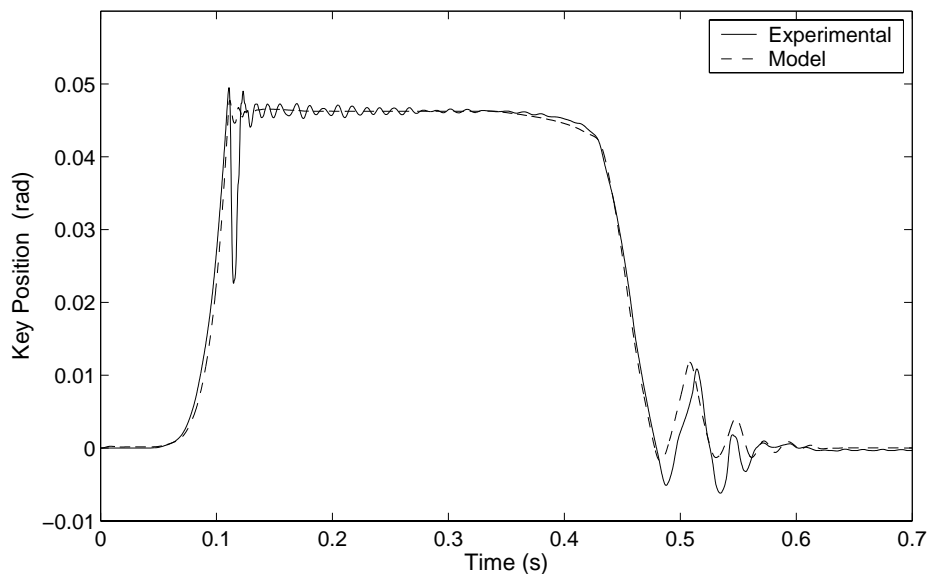


Figure 4.2: Experimental and Model Rotation of Key for *Forte* Blow ($\theta_k(0) - \theta_k$)

The rotational positions of the key, whippen, and hammer during the *forte* blow for the model simulation and experiments are plotted in Figures 4.2, 4.3, and 4.4.

The first thing to note is that from the start of the blow until the hammer strikes the string at 0.11 seconds, the experimental and model results agree very well for all three bodies. This inspires confidence that the model properties that are predominant in high acceleration, such as masses, moments of inertia, and spring forces, accurately represent the system.

As the positions match so closely and string impact occurs at the same time, it is fair to say that the model is an accurate tool for predicting the velocity of the hammer head.

The model results also look very good after the hammer hits the ‘string’. However, it must be remembered that the damping parameter in the ‘string’ contact was manually adjusted to produce the same rebound speed as the experimental action. String modelling is not considered in this project, and in order to prevent inaccuracies in the string behaviour from influencing the rest of the system, the model was manually adjusted to match the real behaviour.

There is also good agreement in the back check position, the position at which the

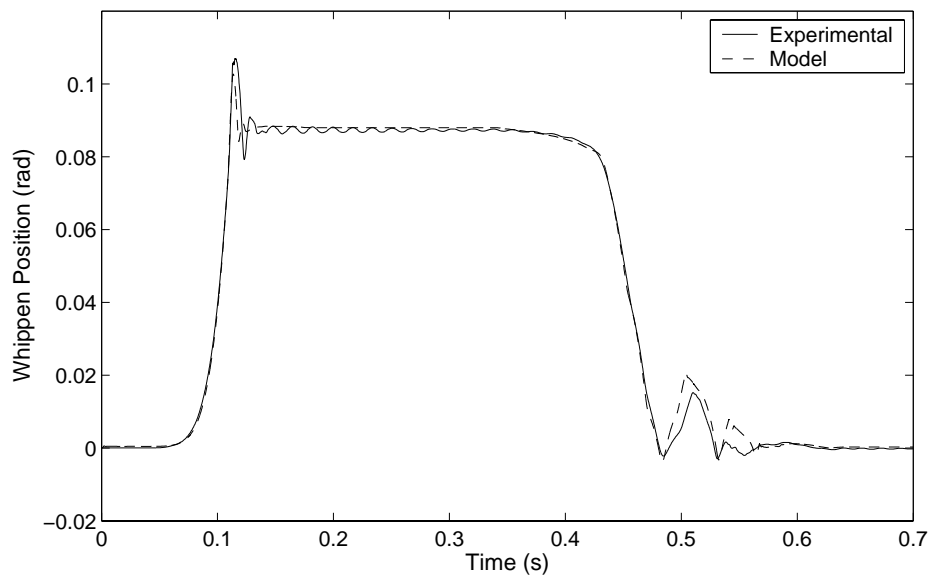


Figure 4.3: Experimental and Model Rotation of Whippet for *Forte* Blow ($\theta_w - \theta_w(0)$)

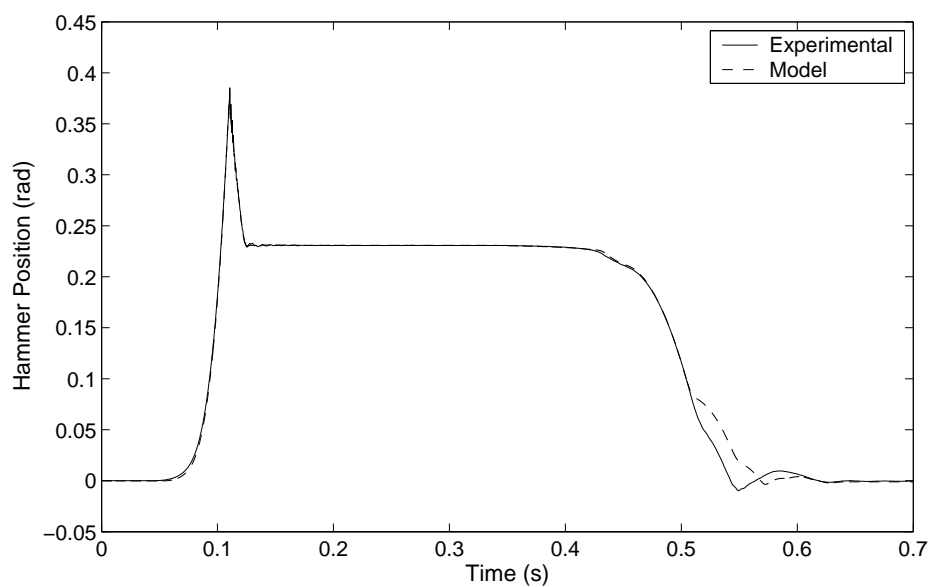


Figure 4.4: Experimental and Model Rotation of Hammer for *Forte* Blow ($\theta_h(0) - \theta_h$)

hammer stops after rebounding from the ‘string’. This agreement is a good indication that the regulation process was performed properly, as this is one of the parameters that was adjusted, as discussed in Section 2.3.

After 0.11 seconds there are several discrepancies that must be addressed. First, it is worth noting that the experimental results show a significant oscillation in the key and whippen. This was investigated with high speed video, and while the videos themselves can not be included in the thesis, they provided confirmation of the cause of the oscillations.

When the hammer bounces off the ‘string’, there is a significant vibration in the head due to the flexibility in the hammer shank. While there is a small noticeable vibration in the hammer rotation, the amplitude is small compared to the large scale of rotation on the plot. This vibration is not transmitted through the knuckle to the whippen, but causes a significant oscillation in the key once the hammer contacts the back check. This vibration is also visible in the whippen, which is simply resting on the key at this time. This oscillation is not present in the model results, since the model does not include any flexible bodies.

A second discrepancy is seen in the key rotation once it reaches its bottom at 0.11 seconds. The downward spike seen in the experimental position is caused by an erroneous measurement by the encoder, as discussed in Section 3.2.2. Similar errors appear at 0.48, 0.53, and 0.56 seconds. While there really is bouncing in the experimental results, the three low spikes are somewhat lower than they should be. In the experimental action, the bounces are also somewhat slower, since it takes some time for the key to return to the balance rail after bouncing up.

This lifting at the balance rail causes problems because it causes erroneous readings, but also because it allows motion in the key that is not permitted by the perfect revolute joint in the model.

A third discrepancy appears at 0.50 seconds, after the key is released. At this time, the rotation of the experimental hammer keeps decreasing while the model hammer is slowed down and the two curves diverge.

Shortly before that time, the key was released and all three bodies were allowed to fall. The key and whippen fall sooner than the hammer and bounce off the key bed. Meanwhile, the hammer is free-falling.

The key and whippen seem to bounce slightly sooner in the model, and this causes the hammer to reconnect with the whippen sooner in the model than in the experiment. This causes the model hammer to slow down sooner, and diverge slightly from the experimental action. This is an example of how a small difference in the behaviour of one component can significantly affect the behaviour of another. In complicated systems with several bodies bouncing off each other, this sensitivity to error is to be expected.

4.2 Piano Blow

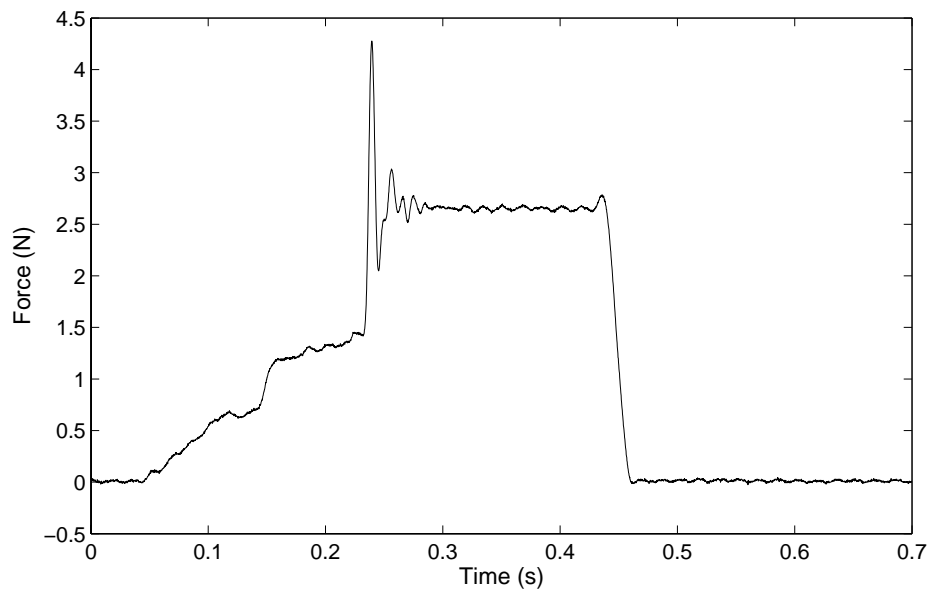
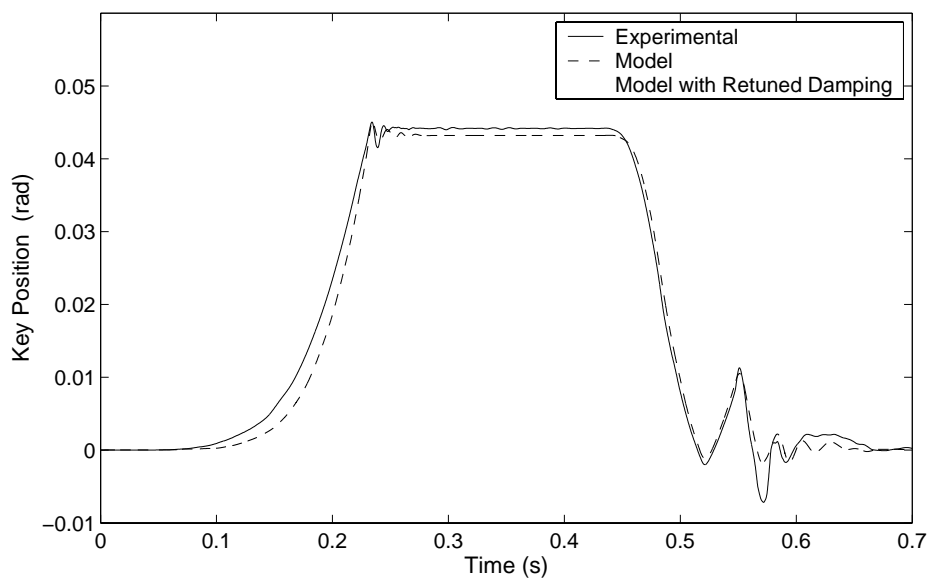
4.2.1 Contact Model with *Forte* Calibration

While the damping factors in the contact model were calibrated to be accurate at speeds normally seen in a *forte* blow, it is also important to see how the model responds to different blows. The model and experimental results were also compared for a *piano* blow. Only the force profile was changed. The regulation was not performed before these trials.

The force profile used for the *piano* blow, as measured in Section 3.2.1, is shown in Figure 4.5. This profile starts at 0 and gradually increases to about 1.5 N before spiking when hitting the key bottom. This force profile is a similar shape as the *forte* profile, though the magnitude of the force is about seven times less, and the *piano* profile requires about three times longer to reach the key bottom.

This profile has a very noticeable oscillation throughout. This is likely due to noise in the load cell measurement from surrounding power wiring, since the oscillation is exactly 60 Hertz. This oscillation may have been present in the *forte* profile, but was not visible due to the much larger scale of the force.

The rotational positions of the key, whippen, and hammer are plotted in Figures 4.6, 4.7, and 4.8. The results are close, especially considering that the damping in the contact model is tuned to the contact speeds when the forces are seven times higher than those present in a *piano* blow. While the graphs are not as similar as the *forte* trials, the model results follow the experimental results very well. This would indicate that while the damping in the model has some impact on the overall behaviour, the model can be used over a wide range of input forces with reasonable results.

Figure 4.5: Force Profile for *Piano* BlowFigure 4.6: Experimental and Model Rotation of Key for *Piano* Blow ($\theta_k(0) - \theta_k$)

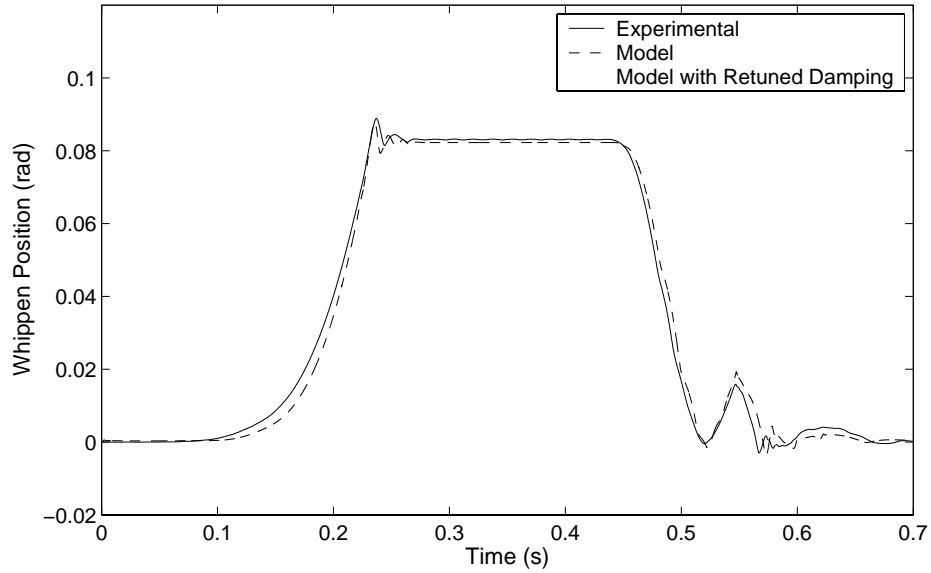


Figure 4.7: Experimental and Model Rotation of Whippet for *Piano* Blow ($\theta_w - \theta_w(0)$)

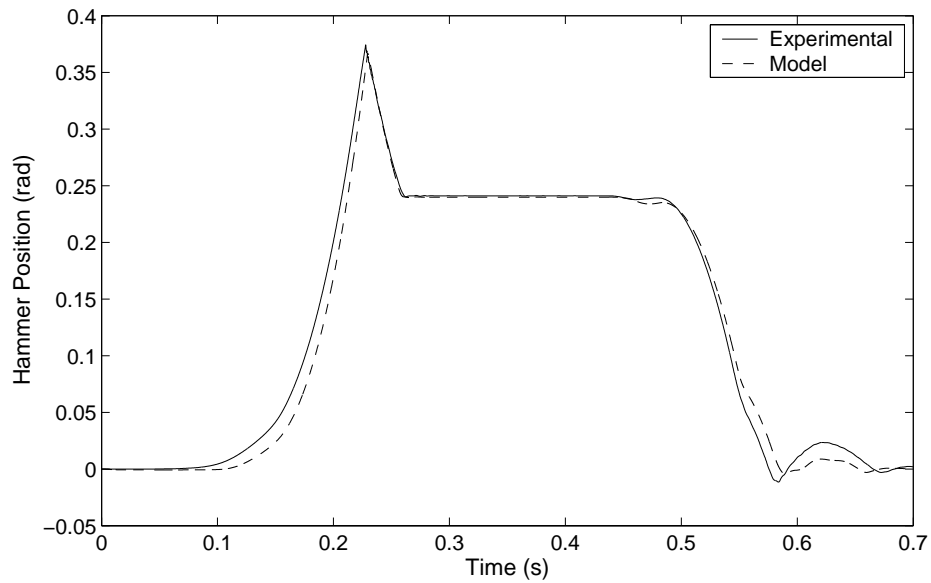


Figure 4.8: Experimental and Model Rotation of Hammer for *Piano* Blow ($\theta_h(0) - \theta_h$)

One of the main differences between the results is that the motion of the model before striking the string is somewhat different than experimental results. The motion of all three components is slightly delayed in the model. This would seem to indicate a more compliant contact. This is as expected because lower speeds in the *piano* blow would cause lower forces in the contact model during compression. If the speeds were higher, or the damping parameters were calibrated for lower speeds, the contacts would appear stiffer during compression.

At the lower speeds in the *piano* blow, the hammer does not oscillate significantly, which allows for much more steady hammer and whippen positions than with the *forte* trial.

These experimental results also do not show a large dip in the key position when the key hits the bottom, indicating that the key does not significantly lift off the balance rail at that time. There is a small lift when the key returns at 0.58 seconds.

4.2.2 Contact Model with *Piano* Calibration

In order to investigate the sensitivity of the action model to the damping parameters, new damping parameters were calculated corresponding to the speeds found in the *piano* blow. The tuning performed on the damping parameters for the *forte* blow was done based on actual speeds measured in the experiment. However, the damping performed for the following trials was done based on speeds measured from the model results for a *piano* blow. This makes the following results less legitimate than the previous, since the previous model parameters were completely derived from the experimental system. However, the following results will still provide some indication of how more reasonable damping parameters affect the behaviour of the model.

The new contact parameters that were calculated with the lower speeds of the *piano* blow were around four to five times larger than the *forte* blow, indicating that the model will now have similar contact behaviour at four to five times lower speeds.

Figures 4.9, 4.10, and 4.11 are the same as the previous Figures 4.6, 4.7, and 4.8, except that they now include the results from the model with retuned damping parameters. It seems that retuning the damping parameters has very little effect on the behaviour of the system. The results are nearly identical to the positions of the model with the damping

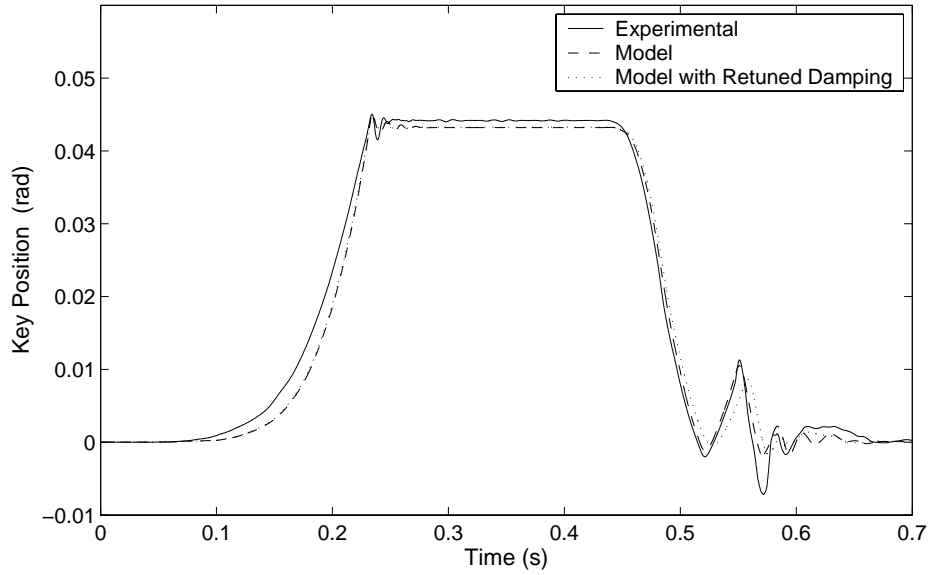


Figure 4.9: Model Rotation of Key with Increased Damping for *Piano* Blow ($\theta_k(0) - \theta_k$)

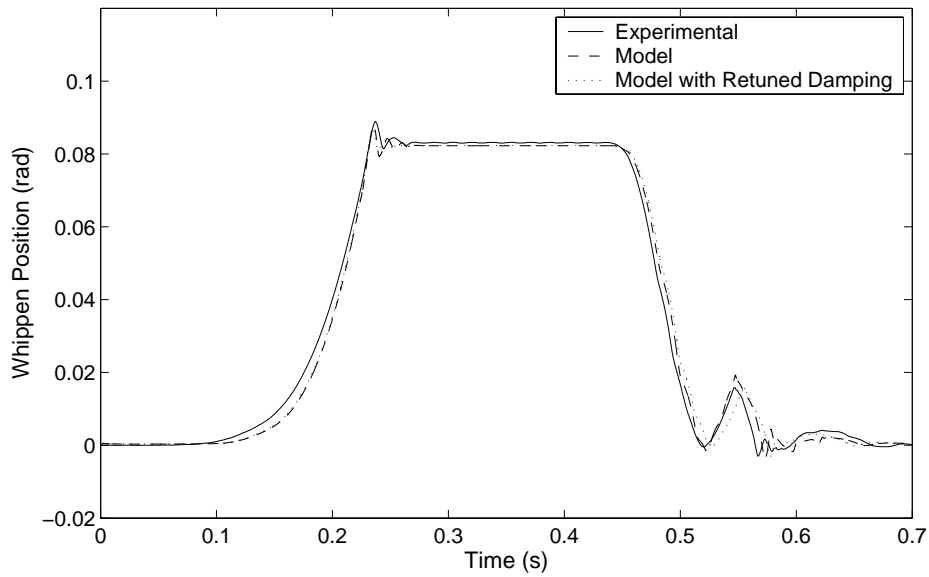


Figure 4.10: Model Rotation of Whippen with Increased Damping for *Piano* Blow ($\theta_w - \theta_w(0)$)

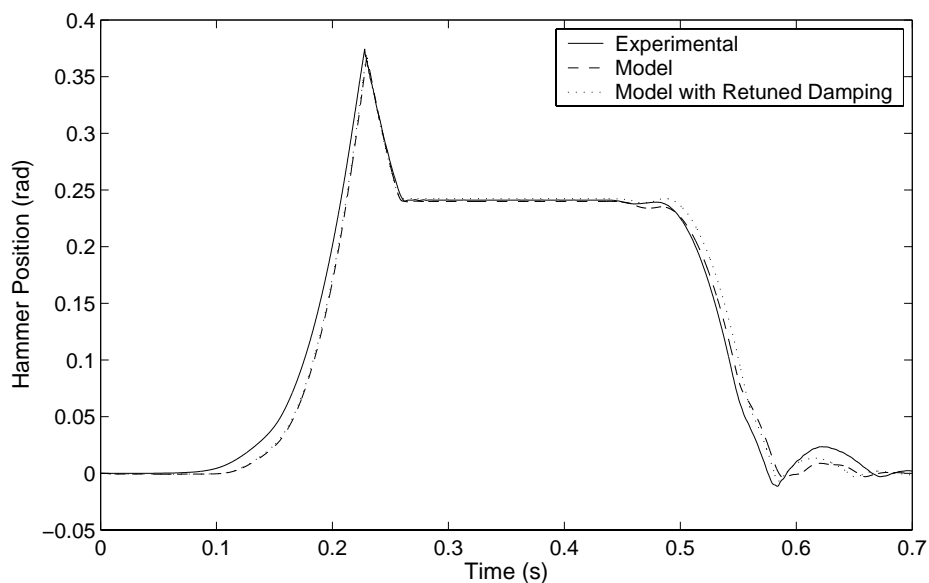


Figure 4.11: Model Rotation of Hammer with Increased Damping for *Piano* Blow ($\theta_h(0) - \theta_h$)

calibrated to *forte* speeds.

Based on these results, it would seem that the model results are not very sensitive to the damping in the contacts, though this is investigated further in later sections.

It was previously hypothesized that the discrepancy in the behaviour of the model for a piano blow was due to the tuning in the damping of the contact model. However, after retuning the damping parameters, the same discrepancy exists, indicating that the previous explanation is not correct.

Another possible explanation is that the force/displacement curves used in the contact model (the spring part of the contact) were measured for the peak forces that appear with a *forte* blow. While the loading portion of the curves should be the same, the unloading curves would be different with lower peak forces.

Also, it might be that the inaccuracies that cause the discrepancies in the *piano* results are also present in the *forte* results, but they are less significant because of the larger forces. Effects such as friction might be more significant at lower forces.

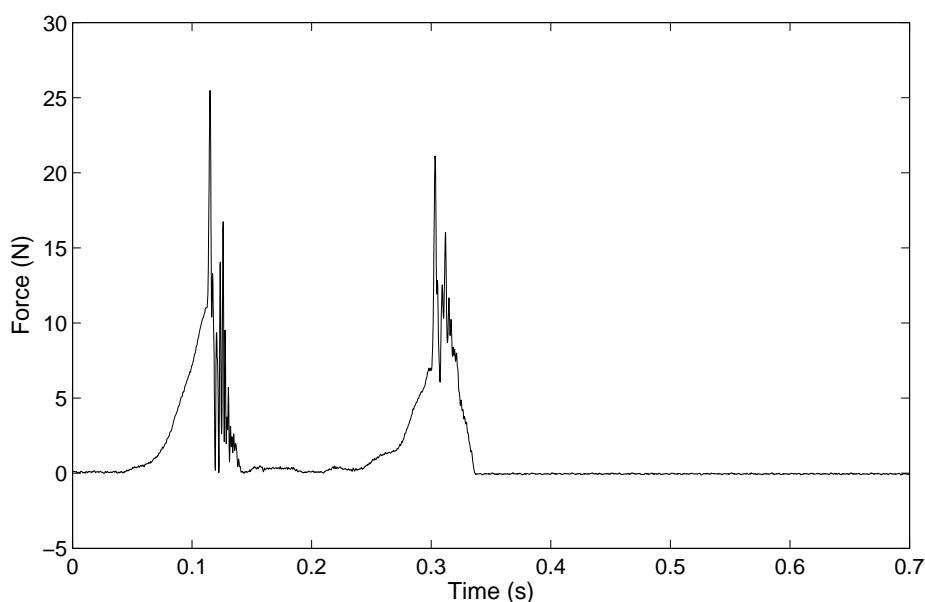


Figure 4.12: Force Profile for Double Blow

4.3 Double Blow

In order to test the model in a more difficult situation, a double blow profile was created, as shown in Figure 4.12. The profile was created by combining two *forte* blows 0.20 seconds apart. This should represent a pianist playing the same note twice rapidly.

It was expected that the behaviour of the model under a double blow would be harder to simulate. With a double blow, the action undergoes a far more complex motion, and since any difference between model and experimental results will be amplified through the simulation, the behaviour in the later parts of the simulation is expected to show more discrepancies.

The rotational positions of the key, whippen, and hammer during the double blow are plotted in Figures 4.13, 4.14, and 4.15. As with the *forte* trials, the behaviour of the model during the initial strike matches the experimental results very closely. However, after that time, there is a significant difference in the results.

It appears that the model action recovers to its initial position much sooner after the first blow than the experimental action. As a result, the second blow is initiated in a

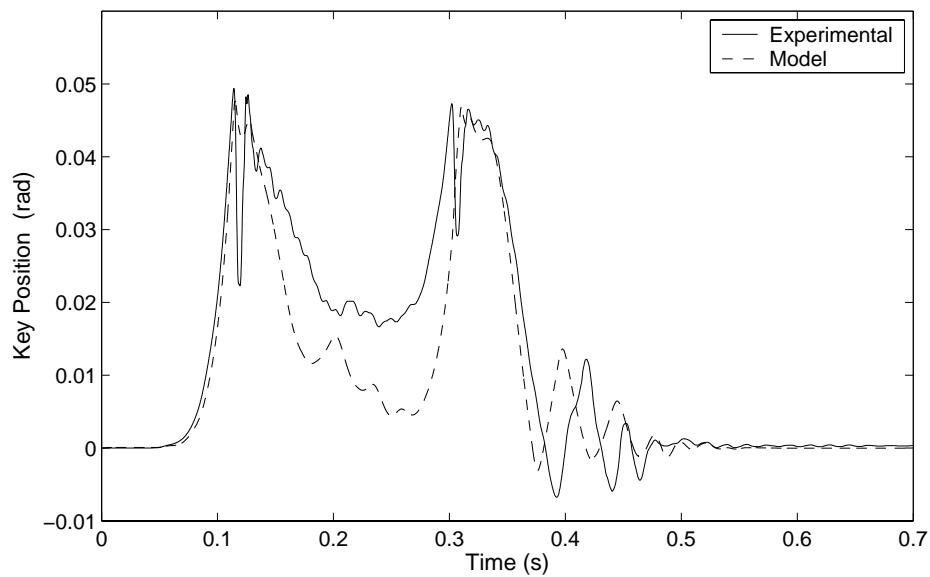


Figure 4.13: Experimental and Model Rotation of Key for Double Blow ($\theta_k(0) - \theta_k$)

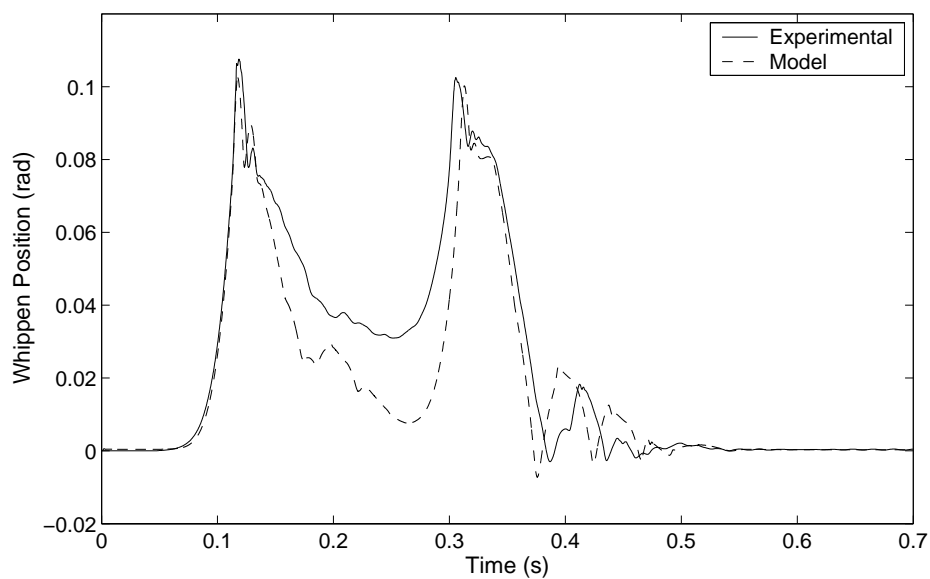


Figure 4.14: Experimental and Model Rotation of Whippen for Double Blow ($\theta_w - \theta_w(0)$)

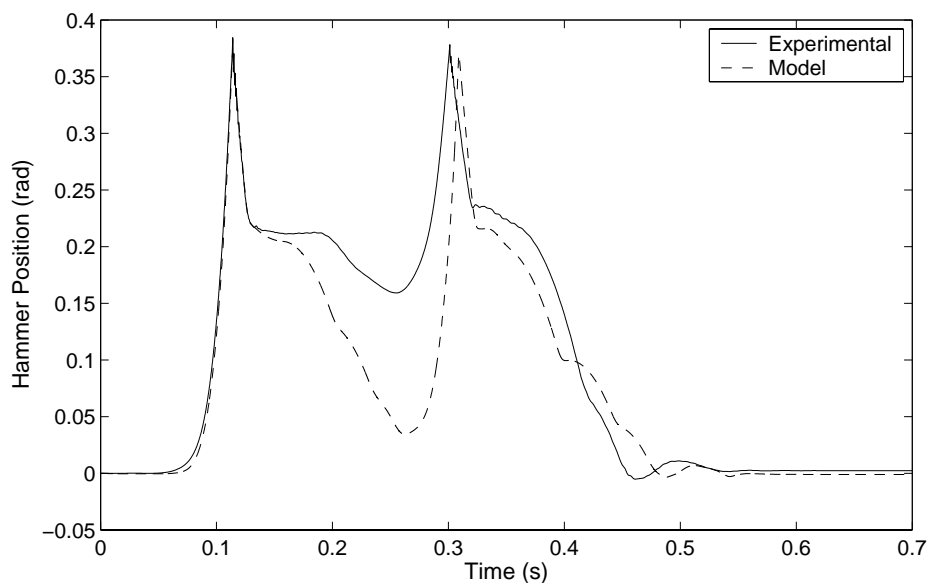


Figure 4.15: Experimental and Model Rotation of Hammer for Double Blow ($\theta_h(0) - \theta_h$)

different state and the model action has farther to travel before the hammer strikes the string.

As the recovery of the action (the time between the two blows) occurs with very little force applied at the key front, the behaviour is mostly dependent on the friction in the action. This would indicate that the friction in the model action is too low, or that there is some friction in the experimental action that is not modelled. This low friction is less significant under the high forces that occur in a single *forte* blow, but are more important during the *piano* blow, which has lower forces, and the double blow, which has longer periods of time when the bodies are allowed to move freely with no force applied.

4.4 Sensitivity Investigations

Several experimental trials were performed to investigate the sensitivity of the model to various parameters. While no formal sensitivity analysis procedure was followed, the trials provide some indication of how certain parameters affect the system.

It was observed in Section 4.2 that greatly increasing the damping in the system seemed

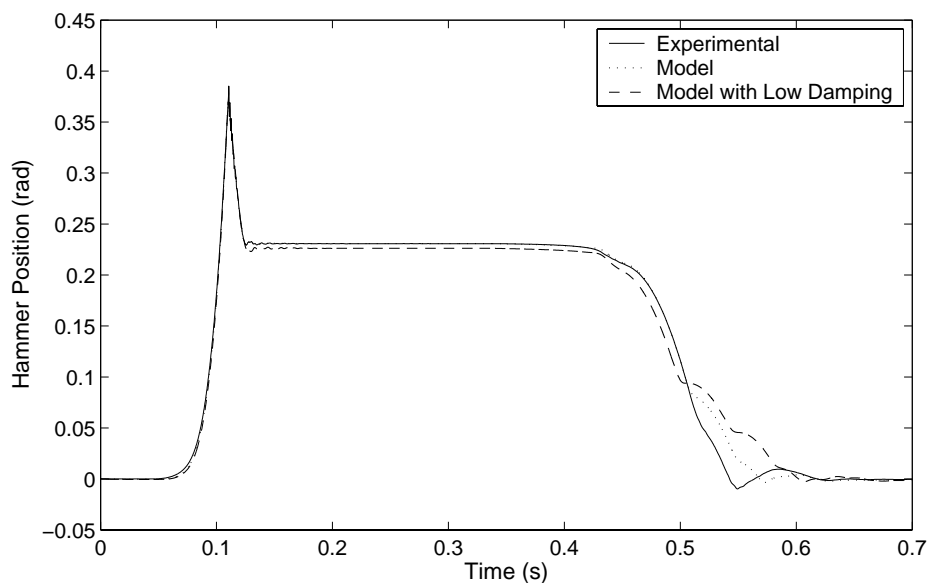


Figure 4.16: Model Rotation of Hammer with Decreased Damping for *Forte* Blow ($\theta_h(0) - \theta_h$)

to have little effect on the behaviour of the action with a *piano* blow. In order to further investigate this, a trial was performed with a *forte* blow on the model with all of the damping parameters in the system (except the ‘string’ contact) reduced by a factor of 10. The resulting hammer position is seen in Figure 4.16.

Reducing the damping in the system has some effect. The hammer checks slightly lower than before, and seems to diverge slightly after the key is released. However, the overall behaviour is still fairly close to the experimental system.

The effect of completely removing damping from the system is seen in Figure 4.17. Completely removing damping from the system has a large effect on the behaviour. The hammer was not properly held on the back check, and instead kept bouncing on the repetition lever. While the damping can be altered significantly without too much difference, eventually it reaches a point where certain parts of the mechanism fail to work properly, then the behaviour diverges radically.

Another trial was performed with all tangential friction removed from the model, which is shown in Figure 4.18. Again, the hammer fails to check properly on the back check. This

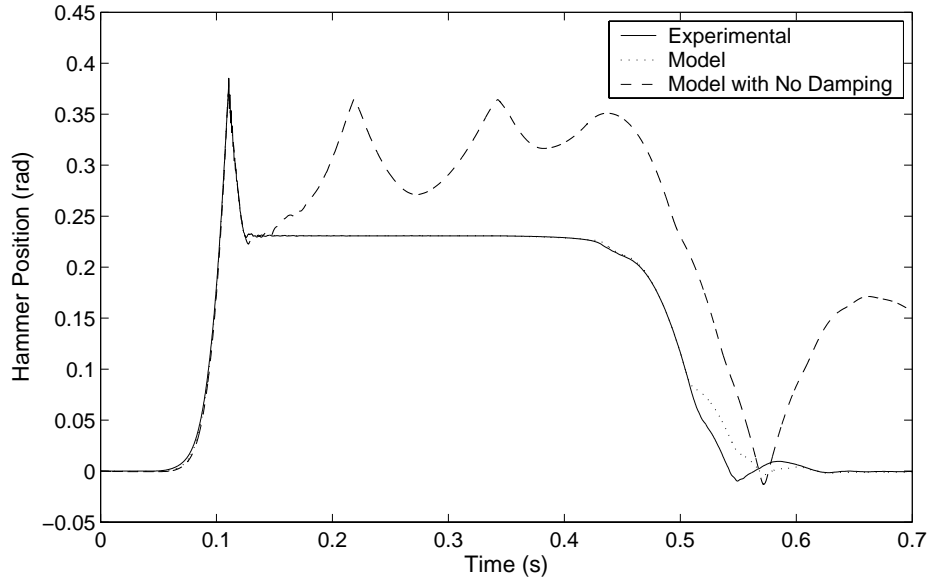


Figure 4.17: Model Rotation of Hammer with No Damping for *Forte* Blow ($\theta_h(0) - \theta_h$)

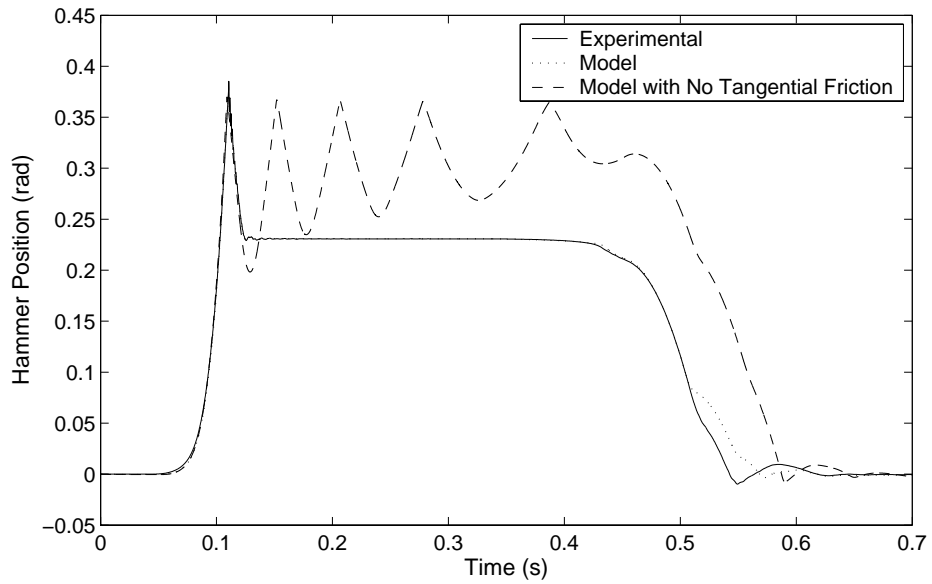


Figure 4.18: Model Rotation of Hammer with No Tangential Friction for *Forte* Blow ($\theta_h(0) - \theta_h$)

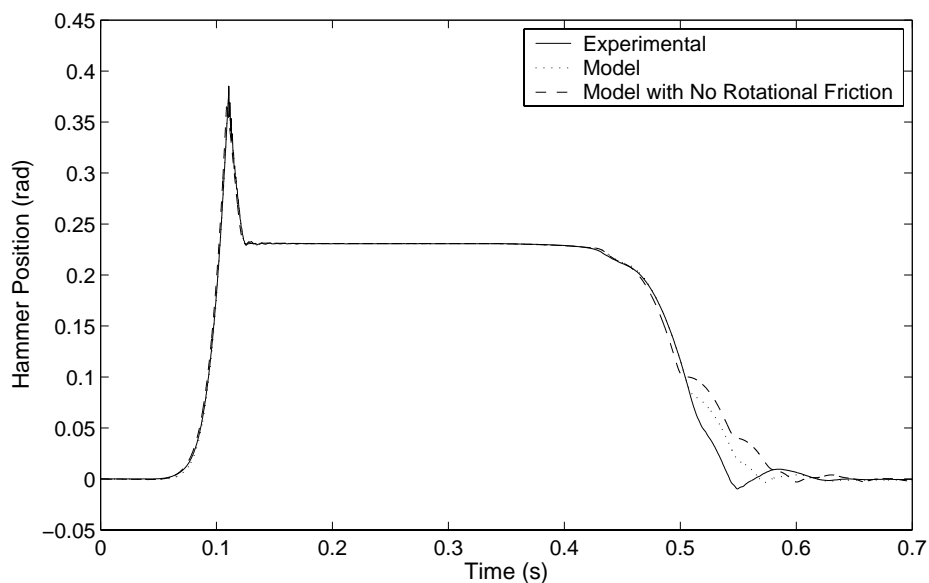


Figure 4.19: Model Rotation of Hammer with No Rotational Friction for *Forte* Blow ($\theta_h(0) - \theta_h$)

is not unexpected, as friction is the only force that will tend to hold the hammer on the check. This indicates that tangential friction (at least in the back check) is critical to the proper behaviour of the system, and the model is capable of accurately predicting this effect.

Finally, a trial was performed with the rotational friction removed from all of the revolute joints. This is plotted in Figure 4.19. This plot indicates only a minor deviation from the normal trial after 0.50 seconds. While it is widely accepted by piano technicians that the friction in the felt bushings is a very important factor in maintaining the right ‘feel’ of an action during soft blows, it seems to have little effect under harder playing.

It is interesting to note that all of these changes to friction and damping have had almost no effect on the behaviour of the system during the initial strike. It would seem that energy loss due to friction and damping is not significant in this phase of the operation. This might explain why previous researchers’ models were able to reasonably model the piano action for the initial strike, even without including damping effects.

However, during the rest of the strike, changing parameters can have a large impact on

the behaviour. As there are many bodies interacting, a small change in force or velocity in one might cause it to miss a contact with another, causing the results to drastically diverge.

Chapter 5

Conclusions and Future Research

5.1 Conclusions

The goal of this project was to create a computer model of a piano action. While many models have been made previously, none had characteristics necessary to be useful as a design and testing tool.

Such a model was created, using a combination of automatically generated dynamic equations produced by *DynaFlexPro* and *Maple*, and ODE solvers and custom contact modelling code in *MATLAB*.

All parameters in the model are directly measured from the physical properties of the action components, including masses, moments of inertia, physical dimensions, friction coefficients, and contact forces. This allows the model to be used to test the design of actions that do not exist, and determine how changing various properties and dimensions would affect the behaviour of an action.

The model is built with a direct correlation between internal variables and physical properties, meaning that internal measurements, like forces and speeds, can be extracted from the model.

In order to verify that the model was able to accurately reproduce the behaviour of an action, an experimental apparatus was set up to take measurements from a real action. The apparatus used a motor to actuate a key, and optical encoders and a high speed video camera to measure the positions of the bodies in the system. The motor was found to create

a very reliable, reproducible force profile on the key. The positions of the bodies measured by the encoders were also extremely repeatable, though there was some inaccuracy in the position of the key at specific points in the blow due to the key bouncing off the balance rail.

A qualitative comparison of the model results and experimental measurements shows that the model is able to reasonably predict the behaviour of a piano action. The correlation between the model results and experimental results is excellent for the whole key blow and release when the action is under high forces, such as during a *forte* blow.

During softer strikes, the model results are still good across the key blow and release, though not as consistent as during harder blows. There is some deviation between model and real behaviour with a double blow, where there is a significant period of time when the key is released and allowed to fall back. The model seems to fall back significantly faster than the real action. This could be an indication that the friction terms in the model are underestimated, since friction effects are more significant during low forces.

Another discrepancy is that the real action undergoes some vibration, primarily due to flexibility in the hammer shank. This oscillation is not visible in the model results, since the model does not consider flexibility in the bodies.

It was found that large changes to friction and damping had little effect on the behaviour of the action with a *forte* blow, until the model reached a point where certain bodies never made contact or friction was insufficient to hold certain bodies together. At that point, the behaviour of the model was drastically different than experimental observations.

5.2 Future Research

The current action model produces reasonable results for many situations. Another important function it has performed is identifying which parts of the piano action model are most important. Several areas were identified where further refinement in the model would improve the results.

As there are noticeable effects in the experimental action caused by flexibility in the hammer shank, this is an obvious area of improvement in the model. Flexibility might also be significant in other bodies, such as the key and whippen. Adding flexible bodies should

be relatively simple, as they are supported by *DynaFlexPro*.

The contact model used in the action model produces reasonable results, but there are some known issues. Mainly, the reaction force produced depends on the speed of the contacting bodies, even though contact experiments have shown that the contact force for felt is not dependent on the contact speed. Other felt contact models could be investigated, along with other methods of modelling hysteretic behaviour, such as the Preisach Model.

While some physical properties of the action (as listed in Appendix A), such as dimensions and masses, were measured accurately, other properties, such as friction, are less reliable. Higher accuracy load measurement devices would be necessary to improve the accuracy of the friction parameters. It is possible that such improved measurements might improve the behaviour of the model during the *piano* blow, as described in Section 4.2.2.

Certain traits of the piano action were not considered in the model. The felt bushings were modelled as perfect revolute joints, though it is known that there is some movement in the bushings. More importantly, the key resting on a balance rail was also modelled as a perfect revolute joint. The translational motion of the key relative to the balance rail caused a noticeable discrepancy in the key position measurement, and the effect of this motion was not considered in the model. Two encoders could be used on the experimental key to accurately read the motion, and the revolute joint on the model key could be replaced with a compressible contact.

The input variable in the model, the force at the key front, is not truly independent, as it depends on the actuation system in the experimental apparatus. This actuation system could be modelled in the future, and perhaps a more independent input variable, such as motor current, could be chosen as an input. It might also be interesting to use an actuation system that more closely resembles the arm and finger of a pianist, though modelling such a system would be difficult.

While the piano string was not considered in this model, an accurate model of hammer and string interaction could be added.

Though it was not considered in this model, aerodynamic effects could be significant, especially for fast moving bodies like the hammer.

Finally, while the purpose of this project was simply to create and test the action model, now that the model is completed, it can be used for further investigations. Trials

and analyses could be performed using the model to investigate some issues that piano technicians regularly face, such as the significance of joint friction at softer blows, and how the ‘feel’ of the action is affected by changes to the action. A more complete sensitivity analysis, or a full system identification procedure, could be performed to determine the importance of certain model parameters.

References

- [1] S. J. Cull and R. W. Tucker. On the modelling of coulomb friction. *Journal of Physics A: Mathematical and General*, 32:2103–2113, 1999.
- [2] G. Van den Berghe, B. De Moor, and W. Minten. Modeling a grand piano key action. *Computer Music Journal*, 19(2):15–22, 1995.
- [3] J. I. Dunlop. On the compression characteristics of fibre masses. *Journal of the Textile Institute*, 74:92–97, 1983.
- [4] G. Gilardi and I. Sharf. Literature survey of contact dynamics modelling. *Mechanism and Machine Theory*, 37:1213–1239, 2002.
- [5] B. Gillespie. Dynamic modeling of the grand piano action. In *Proceedings of the International Computer Music Conference*, pages 77–80, 1992.
- [6] B. Gillespie. *Haptic Display of Systems with Changing Kinematic Constraints: The Virtual Piano Action*. PhD thesis, Stanford University, 1996.
- [7] Y. Gonthier, J. McPhee, C. Lange, and J. C. Piedbœuf. A regularized contact model with asymmetric damping and dwell-time dependent friction. *Multibody System Dynamics*, 11:209–233, 2004.
- [8] I. Hayashi, M. Yamane, and H. Mori. Behavior of piano-action in a grand piano. i. analysis of the motion of the hammer prior to string contact. *Journal of the Acoustical Society of America*, 105(6):3534–3544, 1999.

- [9] K. H. Hunt and F. R. E. Crossley. Coefficient of restitution interpreted as damping in vibroimpact. *Journal of Applied Mechanics*, 42:440–445, 1975.
- [10] P. A. Matveev and A. M. Rymiskij-Korsakov. *Sbornik*, 1937.
- [11] A. Oledzki. Dynamics of piano mechanisms. *Mechanism and Machine Theory*, 7(4):373–385, 1972.
- [12] D. Parlitz, T. Peschel, and E. Altenmüller. Assessment of dynamic finger forces in pianists: Effects of training and expertise. *Journal of Biomechanics*, 31:1063–1067, 1998.
- [13] W. Pfeiffer. *The Piano Key and Whippen*. Verlag Das Musikinstrument, 1967.
- [14] W. Stamm. Compressional behaviour of felts. Master’s thesis, University of Karlsruhe, 2004.
- [15] Steinway and Sons. *Steinway and Sons Technical Reference Guide*, 1992.
- [16] T. N. Topper and B. L. Wills. The computer simulation of piano mechanisms. *International Journal of Modelling & Simulation*, 7(4):135–139, 1987.
- [17] C. M. van Wyk. Note on the compressibility of wool. *Journal of the Textile Institute*, 37:285–292, 1946.

Appendix A

Model Parameters

The following sections list all of the parameters that were used in the action model. Figure A.1 shows all of the points that must be considered in order to model the behaviour of the action. It shows all joints, centres of mass, contact points, and coordinate systems for the five piano action components as well as ground.

A.1 Mass Properties

The masses, mass moments of inertia, and locations of the centres of mass (as defined in Figure A.1) for the five components of the piano action can be seen in Table A.1.

Component	Mass (kg)	Mass Moment of Inertia (kg·m ²)	Centre of Mass (m)	
			x	y
Key	0.12008	2.75E-03	0.0514	0.0158
Whippen	0.01196	1.69E-05	0.0502	-0.0018
Jack	0.00265	7.78E-07	0.0008	0.0195
Repetition	0.00371	4.10E-06	0.0021	-0.0012
Hammer	0.01174	2.90E-05	-0.1022	0.0145

Table A.1: Inertia Properties of Action Components

The mass of each body was measured using a simple lab scale. The centres of mass

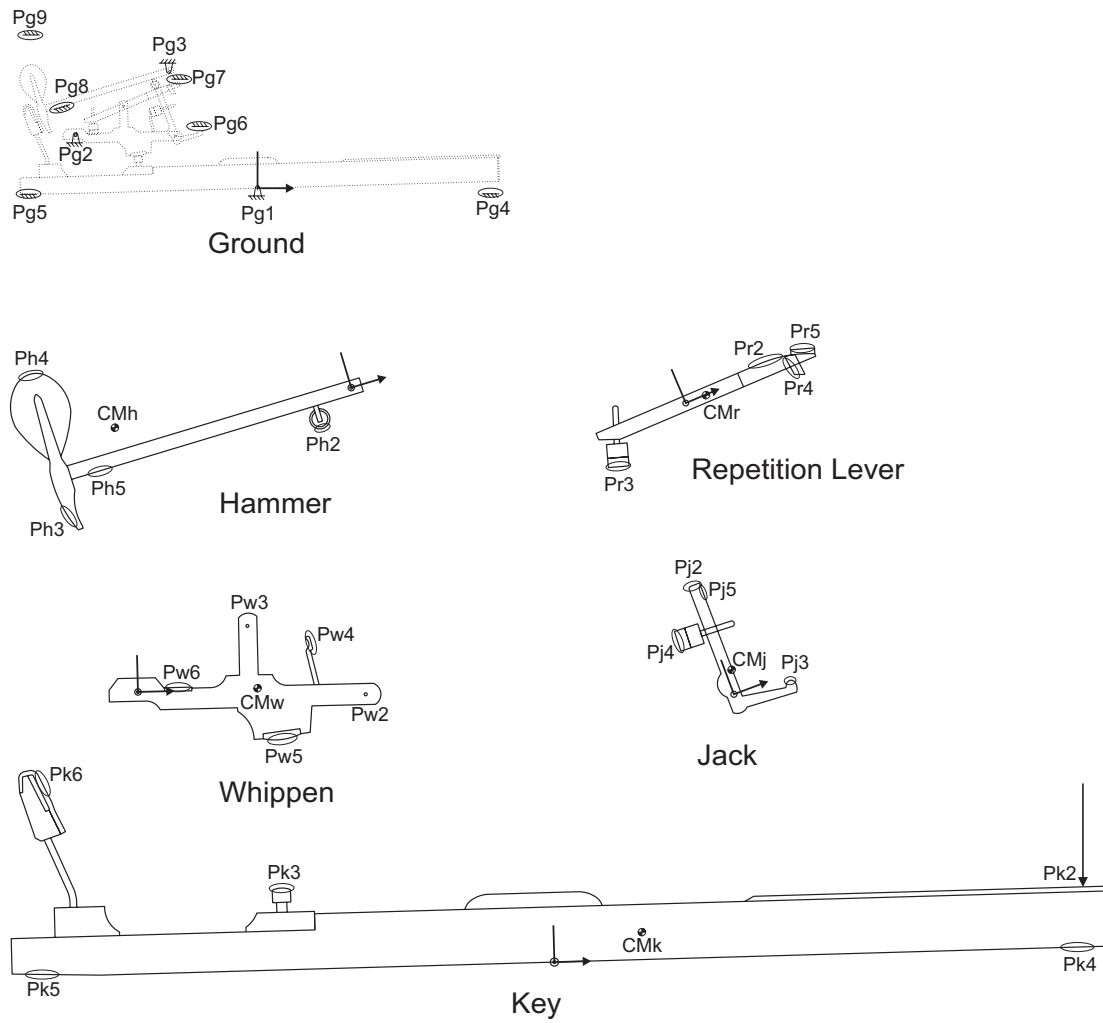


Figure A.1: Defined Points on Action Components

were located by suspending the bodies by a thread from two different points, drawing a vertical line under the fulcrum, and measuring the location of the intersection.

In order to determine the mass moments of inertia, the bodies were suspended from a string and swung like a pendulum. The mass moments of inertia about the pivot point I_p , were then determined from the following expression for the period of a pendulum:

$$I_p = mgl \left(\frac{T}{2\pi} \right)^2 \quad (\text{A.1})$$

where m is the mass of the body, g is the gravitational constant, l is the distance from the pivot point to the centre of mass of the body, and T is the period of oscillation. The moments of inertia about the centre of mass, I_{cm} , were then calculated using the parallel axis theorem:

$$I_{cm} = I_p - ml^2 \quad (\text{A.2})$$

Point	Description	Position (m)		Unit Vector		Radius (m)
		x	y	x	y	
Pg1	Pin Location	0.0000	0.0000			
Pg2	Pin Location	-0.1810	0.0528			
Pg3	Pin Location	-0.0883	0.1166			
Pg4	Circle Contact	0.2172	-0.0077			0.0050
Pg5	Circle Contact	-0.2037	-0.0105			0.0050
Pg6	Line Contact	-0.0580	0.0640	0.000	-1.000	
Pg7	Circle Contact	-0.0843	0.1132			0.0033
Pg8	Circle Contact	-0.1921	0.0766			0.0050
Pg9	Line Contact	-0.2196	0.1706	0.000	-1.000	

Table A.2: Geometric Properties of Ground

A.2 Geometric Properties

All bodies were scanned using a flatbed scanner, and the images were scaled to match known dimensions. The images were then imported into *AutoCAD* where the bodies were traced and the dimensions measured. Ground dimensions were determined the same way, though the initial image was obtained using a digital camera, since the experimental apparatus could not be placed on a flatbed scanner.

Tables A.2, A.3, A.4, A.5, A.6, and A.7 list the coordinates of the key points and describe the contact surfaces for the fixed locations and all of the components of the action. All coordinates are listed in relation to the frame shown on each body in Figure A.1.

All of the contact surfaces in the model are one of three possible two-dimensional geometries:

Circle A simple circular surface defined by the centre of the circle and radius.

Line An infinitely long line defined by a point on the line and a unit normal vector.

Hybrid A shape consisting of an arc segment and two lines extending infinitely from the tangents of the arc. This is described by the centre and radius of the arc, and the

Point	Description	Position (m)		Unit Vector		Radius (m)
		x	y	x	y	
Pk2	Pin Location	0.2278	0.0261			0.0097
Pk3	Circle Contact	-0.1176	0.0259			
Pk4	Line Contact	0.2175	0.0000	0.000	-1.000	
Pk5	Line Contact	-0.2208	0.0010	-0.041	-0.999	
Pk6	Line Contact	-0.2192	0.0817	0.904	0.427	

Table A.3: Geometric Properties of Key

Point	Description	Position (m)		Unit Vector		Radius (m)
		x	y	x	y	
Pw2	Pin Location	0.0989	-0.0035			0.0253
Pw3	Pin Location	0.0483	0.0275			
Pw4	Line Contact	0.0759	0.0189	0.969	0.247	
Pw5	Circle Contact	0.0595	0.0030			
Pw6	Line Contact	0.0170	0.0015	0.000	1.000	

Table A.4: Geometric Properties of Whippen

Point	Description	Position (m)		Unit Vector		Radius (m)	Arc (rad)
		x	y	x	y		
Pj2	Hybrid Contact	-0.0010	0.0495			0.0010	1.571 - 3.142
Pj3	Circle Contact	0.0247	-0.0050			0.0021	
Pj4	Circle Contact	-0.0097	0.0300			0.0050	
Pj5	Line Contact	0.0031	0.0477	1.000	0.000		

Table A.5: Geometric Properties of Jack

Point	Description	Position (m)		Unit Vector		Radius (m)	Arc (rad)
		x	y	x	y		
Pr2	Hybrid Contact	0.0363	-0.0521			0.0552	1.300 - 1.571
Pr3	Circle Contact	-0.0361	-0.0093			0.0050	
Pr4	Circle Contact	0.0527	-0.0009			0.0050	
Pr5	Line Contact	0.0561	0.0017	0.317	0.948		

Table A.6: Geometric Properties of Repetition Lever

Point	Description	Position (m)		Unit Vector		Radius (m)
		x	y	x	y	
Ph2	Circle Contact	-0.0170	-0.0091			0.0044
Ph3	Circle Contact	-0.0813	-0.0025			0.0549
Ph4	Circle Contact	-0.1321	0.0356			0.0102
Ph5	Line Contact	-0.1100	-0.0031	0.000	-1.000	

Table A.7: Geometric Properties of Hammer

starting and ending angles of the arc, as measured counter-clockwise from the positive x-axis.

A.3 Contact Properties

The contact parameters for all 13 contact locations are listed in Table A.8.

Contact #	Points		Curve Parameters			Damping Factor	Friction Parameters		
			a	b	c		A	B_1	B_2
1	Pk3	Pw5	1.26E+10	3.26E+07	7.92E+03	1.877	0.167	0	1
2	Pk4	Pg4	4.41E+10	-1.02E+07	1.57E+04	1.219	0	0	0
3	Pk5	Pg5	2.42E+10	-1.11E+07	6.54E+03	2.502	0	0	0
4	Pk6	Ph3	5.86E+11	-3.70E+07	3.11E+04	2.446	0.434	1.78	1
5	Pw4	Pj4	5.28E+09	-7.54E+05	4.42E+03	5.781	0	0	0
6	Pw6	Pr3	2.53E+10	-9.89E+06	7.07E+03	7.732	0	0	0
7	Pj2	Ph2	3.92E+11	1.10E+07	3.23E+04	4.694	0.177	1.85	1
8	Pj3	Pg6	7.46E+10	-2.29E+07	1.32E+04	1.527	0	0	0
9	Pj5	Pr4	6.02E+10	-1.68E+07	6.96E+03	0.779	0	0	0
10	Pr2	Ph2	1.09E+12	-7.51E+07	2.23E+04	2.935	0.332	0.73	1
11	Pr5	Pg7	8.82E+11	-7.59E+07	1.67E+04	4.985	0	0	0
12	Ph4	Pg9	1.81E+10	8.19E+07	1.16E+04	0.175	0	0	0
13	Ph5	Pg8	8.58E+08	-1.11E+06	2.39E+03	8.964	0	0	0

Table A.8: Contact Properties

The *Curve Parameters* define the three polynomial terms of the fit curve of Equation (2.5). This curve and the *Damping Factor* are used in Equation (2.4). The procedure used to determine these parameters is discussed in Section 2.2.3.

The three *Friction Parameters*, which are derived from the static and kinetic coefficients of friction, are used in Equation (2.10). The coefficients of friction for each pair of contacting bodies were measured by holding the first body fixed, pushing the second body into the first with a known force, then measuring the force required to start the bodies sliding, and keep them sliding.

A.4 Other Properties

In addition to the mass, geometric, and contact properties already listed, the model also incorporates rotational springs and friction in the revolute joints of the action bodies.

The spring force in the jack was measured to be approximately constant at 0.0042 N·m. The spring force in the repetition lever follows the standard linear spring model with values as shown in Equation (A.3):

$$T = -0.073(\theta_r - 0.832) \quad (\text{A.3})$$

where T is the torque acting on the revolute joint (in N·m), and θ_r is the angle between the repetition lever and the whippen (in radians).

The friction parameters for the revolute joints of the five bodies, as defined in Equation (2.12), are listed in Table A.9.

Component	A	B_1	B_2
Key	0.0122	0	0
Whippen	0.000397	0	0
Jack	0.000397	0	0
Repetition	0.00247	0	0
Hammer	0.00101	0	0

Table A.9: Rotational Friction Parameters

The rotational friction parameter, A is derived directly from the kinetic frictional torque in the joint. This torque was determined by measuring the force required to rotate the joint at a known distance from the the centre of the joint. Static friction, as described by B_1 and B_2 , was not included in these joints.

Appendix B

Experimental Equipment

The following tables list the software and equipment used with the experimental piano action.

Vendor	Package	Version
Kollmorgen	ServoStar MotionLink	4.4.6
National Instruments	LabVIEW Express	7.0
Photron	Motion Tools	1.0.5

Table B.1: Software

Vendor	Part	Description
Kollmorgen	MT308A1	DC Brushless Servo Motor
Kollmorgen	CE03250	DC Brushless Servo Drive, 3 Amp
National Instruments	PCI-7342	Servo/Stepper PCI Motion Controller

Table B.2: Actuation Equipment

Vendor	Part	Description
Sensotec	Model 13, 25 lb	Subminiature Strain Load Cell, 25 pound
National Instruments	PCI-6034E	Multifunction PCI IO Board
National Instruments	SCXI-1520	SCXI Strain/Bridge module

Table B.3: Load Measurement Equipment

Vendor	Part	Description
MicroE Systems	M1510S-40	Digital Encoder Sensor
MicroE Systems	R3213	Encoder Rotary Scale, 1.25 inch
MicroE Systems	R5725	Encoder Rotary Scale, 2.25 inch
National Instruments	PCI-6602	Counter/Time PCI Board

Table B.4: Position Measurement Equipment

Vendor	Part	Description
Photron	FASTCAM-X 1280 PCI	High Speed Video System, 1,280 x 1,024 pixel

Table B.5: High-Speed Video Equipment